

1 **Modelling earthquake rupture rates in fault systems for seismic hazard assessment:**
2 **the Eastern Betics Shear Zone.**

3 Octavi Gómez-Novell^a, Thomas Chartier^{b,c}, Julián García-Mayordomo^d, María Ortuño^a,
4 Eulàlia Masana^a, Juan Miguel Insua-Arévalo^e, Oona Scotti^c

5 **Corresponding author:** Octavi Gómez-Novell^a (octgomez@ub.edu)

6 ^a RISKNAT Group, GEOMODELS, Departament de Dinàmica de la Terra i de l'Oceà,
7 Facultat de Ciències de la Terra, Universitat de Barcelona, 08028 Barcelona, Spain

8 ^b Laboratoire de Géologie, CNRS UMR8538, Ecole Normale Supérieure, PSL University,
9 24 rue Lhomond, 75005 Paris, France

10 ^c Institut de Radioprotection et de Sûreté Nucléaire, 31 avenue de la Division Leclerc,
11 92260 Fontenay aux Roses, France.

12 ^d Instituto Geológico y Minero de España, 28760 Tres Cantos, Spain.

13 ^e Departamento de Geodinámica, Estratigrafía y Paleontología, Facultad de Ciencias
14 Geológicas, Universidad Complutense de Madrid, 28040 Madrid, Spain.

15 **Emails:** Octavi Gómez-Novell: octgomez@ub.edu; Thomas Chartier:
16 chartier@geologie.ens.fr; Julián García-Mayordomo: julian.garcia@igme.es; María
17 Ortuño: maria.ortuno@ub.edu; Eulàlia Masana: eulalia.masana@ub.edu; Juan Miguel
18 Insua-Arévalo: insuarev@geo.ucm.es; Oona Scotti: oonascotti@irsn.fr

19 **Declarations of interest:** none

20 **Abstract**

21 Earthquake surface fault ruptures can show very complex geometries and involve
22 different faults simultaneously. Consequently, modern fault-based probabilistic seismic
23 hazard assessments (PSHA) need to account for such complexities in order to achieve
24 more realistic modellings that treat fault systems as a whole and consider the occurrence
25 of earthquake ruptures as aleatory uncertainties. We use SHERIFS, a recent approach of
26 modelling annual rates of complex multi-fault ruptures, to obtain system-level
27 magnitude-frequency distributions (MFDs) for the Eastern Betics Shear Zone (EBSZ,
28 Spain) considering four fault rupture hypotheses. We then analyze the consistency of each
29 scenario based on data from the earthquake catalogue and paleoseismic studies. The
30 definition of the different rupture hypotheses was discussed within the frame of
31 Fault2SHA ESC working group and critical fault input data is extracted from previous
32 published studies. The four rupture hypotheses are defined as incremental scenarios based
33 on fault geometry and kinematics, with lengths varying from minimal fault sections to a
34 rupture of nearly the whole system.

35 The results suggest that multi-fault ruptures involving lengths up to single to several
36 whole faults are consistent with the annual rates from both the instrumental catalogue and
37 paleoseismic record. The method does not allow to completely discard any hypothesis,
38 but it allows to weight the different models in a logic tree for seismic hazard assessment.
39 The approach is revealed as a practical tool for obtaining fault-system MFDs and as a
40 useful tool for highlighting limitations and uncertainties in geological and paleoseismic
41 data to be assessed. This study aims to constitute a step forward in the consideration of
42 complex multi-fault ruptures for future seismic hazard assessments in the region.

43

44 **Keywords**

45 Seismic hazard; fault rupture; annual earthquake rate; paleoseismology; MFD;

46 Gutenberg-Richter

47 **1. Introduction**

48 Characterizing faults as seismogenic sources in probabilistic seismic hazard assessment
49 (PSHA) is far from trivial. Field data shows that earthquake surface ruptures can be very
50 complex, involving faults with different characteristics in a broad system (e.g., 2010 El
51 Mayor Cucupah earthquake; Wei et al., 2011 and 2016 Kaikoura earthquake; Kearse et
52 al., 2018). Modern fault-based PSHA models should then evolve and consider
53 earthquakes corresponding to single-fault ruptures as well as to multi-fault ruptures that
54 propagate through a fault system. In this sense, the occurrence of earthquake ruptures
55 should be treated as an aleatory uncertainty linked to the randomness of the seismic
56 process while exploring the epistemic uncertainty of which rupture is considered in each
57 model.

58 Generally, seismic hazard studies have estimated earthquake parameters from
59 instrumental or historical seismicity data, but classically, the use of fault geological data
60 has not been widespread in source modelling (e.g. Bayrak et al., 2009), mainly due to the
61 lack of good quality input data and efficient modelling tools. The inclusion of faults into
62 seismic hazard calculations has been the subject of many studies as more geological
63 results on the seismic behavior of active faults have become available. Most studies
64 consider faults as independent sources, which accommodate the largest earthquakes from
65 a cut-off magnitude, while the smaller ones occur in a defined buffer zone (e.g. Frankel,
66 1995 in USA; Woessner et al., 2015 in the European SHARE project; Valentini et al.,
67 2017 in central Italy). Geological, paleoseismological and geometrical characteristics of
68 these faults are used to estimate the maximum magnitude (M_{\max}) and the magnitude-
69 frequency distribution (MFD) for each fault in the system, either following an exponential
70 model (i.e., a Gutenberg-Richter distribution; Gutenberg & Richter, 1944) or a
71 characteristic earthquake model (Wesnousky, 1986; Youngs and Coppersmith, 1985).

72 These approaches do not contemplate the occurrence of linked fault ruptures nor the
73 inclusion of fault complexity into the models. However, recent studies have developed
74 system level approaches considering faults as interacting sources that can get involved in
75 linked ruptures and taking into account fault complexities such as geometrical and slip
76 rate variations. In addition, some of these studies consider the occurrence of multi-fault
77 ruptures as an aleatory uncertainty linked to the randomness of the seismic process (e.g.
78 Chartier et al., 2019, 2017; Field et al., 2014; Working Group On California Earthquake
79 Probabilities, 2003).

80 The Eastern Betics Shear Zone (EBSZ; De Larouzière et al., 1988) is the longest active
81 fault system in the Betic Cordillera (SE Spain; Fig. 1a, b) and one of the most seismically
82 active areas in Spain (García-Mayordomo et al., 2007). From a global perspective, it is
83 an area with low-to-moderate seismicity. However, the slip rates estimated for some faults
84 ($> 1 \text{ mm}\cdot\text{yr}^{-1}$; Echeverria et al., 2015; Ferrater, 2016; Ferrater et al., 2017) underline the
85 moderate-high seismic potential of the area and highlight the need to better constrain the
86 probability of occurrence of potentially damaging earthquakes. The EBSZ is a complex
87 fault-system composed by an ensemble of faults with contrasting geometries and slip rate
88 variations (Ferrater et al., 2017).

89 In past PSHA studies, the EBSZ has been modelled as a source zone following the
90 Cornell-McGuire methodology (Cornell, 1968; McGuire, 1976), delineating the territory
91 in zones and obtaining a magnitude-frequency distribution (MFD) from the earthquake
92 catalogue of the area (Gaspar-Escribano et al., 2015, 2008). Other studies have modelled
93 PSHA in terms of Arias intensity (e.g. Peláez et al., 2005). Later on, it has been modelled
94 incorporating major faults as a set of independent segments, considering either a
95 characteristic earthquake model (e.g. Wesnousky, 1986) or an exponential MFD based
96 on geological data (e.g. fault dimensions and slip rate; García-Mayordomo, 2005; García-

97 Mayordomo et al., 2007). For the official seismic hazard map of Spain (IGN-UPM
98 working group, 2013) the EBSZ was modelled as a seismogenic zone, consistently with
99 the zoning model used in the rest of Spain, because at that time the available fault data
100 was neither representative or complete for the whole territory (García-Mayordomo,
101 2015). More and higher precision paleoseismic parameters are available nowadays thanks
102 to several paleoseismic studies conducted in the last decade (e.g. Ferrater, 2016; Insua-
103 Arévalo et al., 2015; Martín-Banda et al., 2015; Martínez-Díaz et al., 2018). Recently,
104 Rivas-Medina et al. (2018) proposed a hybrid approach that avoids setting an arbitrary
105 cut-off magnitude for distributing seismic moment between faults and zones and, at the
106 same time, ensure that this distribution of seismic potential is not double-counted. This
107 is achieved by computing and distributing the seismic potential between faults and zones
108 using the events contained in the completeness period of the catalogue for different
109 magnitude ranges. However, so far no attempts have been done to address and model the
110 occurrence of multi-fault ruptures at the EBSZ with a system-level approach, as we
111 present.

112 In this work, we use the SHERIFS code (Seismic Hazard and Earthquake Rates in Fault
113 Systems; Chartier et al., 2019) to generate synthetically derived MFDs for different fault
114 and multi-fault rupture hypotheses or scenarios at the EBSZ and considering the
115 occurrence of such possible ruptures in each hypothesis as an aleatory uncertainty. The
116 aim of the study is to compare the synthetic MFDs with respect to the earthquake rates
117 calculated using the earthquake catalogue and paleoseismic data. The fit between the
118 modelled rates and the rates from the data can be used as criteria for weighting the
119 different input hypotheses for PSHA. To do so, we first define and explore four fault and
120 multi-fault rupture hypotheses or scenarios at the EBSZ and we use geological fault data
121 from previous published studies as inputs for the calculations, filtered after a thorough

122 discussion (extended in the Appendix). The identification of the epistemic uncertainties
123 related to the definition of the input hypotheses and the discussion of the reliability of the
124 fault data are further objectives of this paper, since these affect the results. It should be
125 acknowledged that the input hypotheses presented here are based on expert criteria and
126 that geological fault data are not always conclusive, hence expert decisions needed to be
127 taken in some cases.

128 The approach used is an alternative to other studies that model earthquake recurrence
129 considering fault data and its uncertainties (e.g. Wang et al., 2012). The rupture rates
130 calculated and discussed in this study as well as the weighting of the different rupture
131 hypotheses might be useful in future PSHA studies. Also, they might also be used for
132 choosing specific earthquake scenarios for neo-deterministic seismic hazard calculations
133 (NDSHA) (e.g. Magrin et al., 2017; Rastgoo et al., 2018).

134 **2. Geological and seismological setting**

135 The EBSZ is a 400 km long active fault system located in SE Iberia dominated by SW-
136 NE left-lateral strike slip faults, some of which are oblique reverse faults. From SW to
137 NE the main faults in the area are named as (Fig. 1b): Carboneras fault (CF), Palomares
138 fault (PF), Alhama de Murcia fault (AMF), Los Tolloos fault (LTF), Carrascoy fault (CAF)
139 and Bajo Segura fault (BSF) (Alfaro et al., 2012a; Bousquet, 1979; De Larouzière et al.,
140 1988; Insua-Arévalo et al., 2015; Martínez-Díaz et al., 2012a; Masana et al., 2004; Silva
141 et al., 1993; among others). These faults accommodate a large portion of the shortening
142 resulting from the convergence of the African and Nubian plates in Iberia since late
143 Neogene (Bousquet, 1979; Martínez-Díaz, 1998; Masana et al., 2004), estimated in 4 to
144 6 mm·yr⁻¹ following a N150° horizontal shortening direction (Argus et al., 2011; Demets
145 et al., 2010).

146 Several studies at the EBSZ (e.g. Ferrater, 2016; Insua-Arévalo et al., 2015; Martín-
147 Banda et al., 2015; Martínez-Díaz et al., 2018, 2003; Masana et al., 2018, 2004; Moreno,
148 2011; Ortuño et al., 2012) have evidenced the occurrence of recurrent morphogenetic
149 earthquakes. Recent studies have also proposed considerably high slip rate values for
150 some of these faults: $1.0 \pm 0.2 \text{ mm}\cdot\text{yr}^{-1}$ (paleoseismological 3D trenching) and 1.6-1.7
151 $\text{mm}\cdot\text{yr}^{-1}$ (geomorphological analysis) for AMF (e.g. Ferrater, 2016; Ferrater et al., 2017,
152 respectively). Remarkably, for some faults such as the northeastern section of AMF
153 (AMF-4; Table 1), slip rate values are subject to large uncertainties, since they are
154 estimated from long term uplifts (Herrero-Barbero, 2016).

155 The EBSZ is one of the most seismically active areas of Spain and it has produced some
156 of its largest historical events (e.g. 1829 Torrevieja earthquake; Fig. 1b) with important
157 damage effects (e.g. Delgado et al., 2011). In addition, recent earthquakes such as the M_w
158 5.1 ± 0.1 , 2011 Lorca earthquake (IGN-UPM working group, 2013) also caused great
159 damage and related slope effects (Alfaro et al., 2012b). Most of the earthquakes in the
160 EBSZ occur at depths $< 20 \text{ km}$ (Martínez-Díaz, 1998) and some historical events are
161 thought to be caused by its main faults (e.g. BSF for the 1829 Torrevieja event; Alfaro et
162 al., 2012a or AMF for the 1674 Lorca event; Martínez-Díaz et al., 2018). Even though
163 there are not known descriptions of surface ruptures during the historical period,
164 paleoseismic studies have demonstrated the occurrence of at least one historical surface
165 rupturing earthquake along the EBSZ (i.e. 1674 Lorca event; Martínez-Díaz et al., 2018).

166 **3. Datasets and methodology**

167 To accomplish our main objectives, we set up possible multi-fault rupture scenarios in
168 the study area and selected the slip rate data on faults from published studies following a
169 critical revision in specific cases (see Appendix). Then we used the SHERIFS code to

170 model MFDs at the whole EBSZ fault system scale and analyzed the consistency of the
171 models with data from the catalogue and paleoseismic studies.

172 **3.1. Definition of fault rupture hypotheses**

173 We defined four possible fault and multi-fault rupture scenarios for the EBSZ system as
174 sets of incremental fault rupture lengths starting from minimal fault sections, which
175 correspond to the segmentation proposed for each fault in the literature (Fig. 2a). These
176 scenarios represent plausible rupture possibilities according to our criteria and the
177 available data, but other could be tested.

178 The different hypotheses are explorative and the length of ruptures in the different
179 scenarios was defined by imposing selected fault characteristics as barriers for rupture
180 propagation. In our case, only geometry (mainly sense of dip) and kinematic changes
181 between major faults or groups of faults were used as criteria to explore multi-fault
182 rupture propagation in the different hypotheses (see more details on the specific criteria
183 used in section 3.1.1). In the case of AMF though, it was considered that the fault cannot
184 rupture with any fault of the system in any hypothesis, since it dips towards the NE
185 (Martínez-Díaz et al., 2012b) and this makes incompatible its linked rupture with the rest
186 of faults of the system. Other fault parameters frequently used as barriers for fault rupture
187 propagation (e.g. Boncio et al., 2004; Field et al., 2014; Wesnousky, 2008) were not
188 contemplated in this study as we explain below.

189 Changes in strike and distance between faults (gaps, stepovers) were not considered as a
190 limiting factor for rupture propagation, since they are not significant enough, considering
191 the criteria applied in California (UCERF-3; Field et al., 2014). Neither slip rate variations
192 along strike were used as barriers, even if these are important. This is consistent with
193 observations on earthquakes such as the 2016 Mw 7.8 Kaikoura earthquake where more

194 than 20 faults ruptured together, some of them with extremely different slip rates (e.g. 1-
195 $2 \text{ mm}\cdot\text{yr}^{-1}$ for the Papatea fault and $24\pm 12 \text{ mm}\cdot\text{yr}^{-1}$ for the Kekerengu fault; Langridge et
196 al., 2018 and Little et al., 2018, respectively).

197 Finally, the aspect ratios between fault length and width were not taken as a limiting factor
198 for the occurrence of long fault ruptures in our models, since there is not a clear threshold
199 for these parameters in large or extreme events, especially for strike-slip regimes. For
200 instance, the 1906 Mw 7.9 San Francisco earthquake or the 1958 Mw 7.77 Alaska
201 earthquake implied rupture lengths of 470 km and 260 km, respectively (Schwartz, 2018)
202 with seismogenic widths of 12 km (Wells and Coppersmith, 1994) comparable to the
203 EBSZ (Table 1). Also, it can be observed from the regressions in Leonard (2010) that, in
204 strike-slip faults, for rupture lengths > 50 km the width becomes constant at a mean of 17
205 km, but the dataset shows large dispersion in this range and a significant amount of large
206 ruptures (> 100 km long) are found in widths similar to the EBSZ.

207 3.1.1. Fault rupture hypotheses

208 For the modelling we only considered the main active major faults of the area (Fig. 1b),
209 although other minor faults are known and have been studied to different degrees (e.g.
210 faults identified by Pedrera et al., 2012).

211 The major faults considered are divided in shorter sections based on their geometry,
212 geomorphic expression and seismicity in the literature, as well as on their kinematics and
213 activity evidence. Offshore segmentation of CF was adopted from Moreno (2011), while
214 onshore was based on García-Mayordomo (2005), same as for PF. Segmentation of CAF
215 was adopted from Martín-Banda et al. (2015), BSF from Alfaro et al., (2012a) and AMF
216 from Martínez-Díaz et al., (2012b).

217 The segmentation for each of these faults was applied to define the minimal sections
218 (hypothesis 1) that in the subsequent hypotheses are linked to generate larger ruptures;
219 ‘multi-fault ruptures’ henceforth. The fault system geometry considered is shown in
220 figure 2a. Mainly for AMF-1, AMF-2, CF and PF we simplified fault sections with several
221 parallel traces or splays to a single trace representative of the overall geometry (Fig. 1b).
222 This was done because fault branches likely link at depth, as suggested by Martínez-Díaz
223 et al. (2012b) for AMF or Moreno (2011) for CF, and fault parameters of the simplified
224 fault traces result from the merging of the individual fault branches; slip rates of CF,
225 AMF-1 or PF are inferred from geomorphological estimations accounting for all
226 branches. Moreover, in CF they are consistent with geodetic data (Table 1 and Appendix).
227 The main difference between the hypotheses considered is the length of the maximum
228 fault ruptures allowed. One hypothesis considers only single-section fault ruptures and
229 the other three allow multi-fault ruptures at different extents (Fig. 2a):

- 230 - Hypothesis 1 (hyp. 1): The length of the segments in the segmentation from the
231 literature (Table 1) set the maximum length of ruptures (Fig. 2a) and multi-fault
232 ruptures with the neighboring sections are not allowed. This follows the classical
233 segmentation model in which is considered that earthquakes are usually confined
234 within specific segments of a certain fault (Schwartz and Coppersmith, 1984).
- 235 - Hypothesis 2 (hyp. 2): The maximum length of ruptures allowed in this hypothesis is
236 that of complete major faults. Neighboring fault sections can rupture together within
237 a same fault, but complex ruptures between different major faults are not envisaged.
238 For example, the whole CF can rupture at a time, but it cannot rupture with its adjacent
239 section of PF (Fig. 2a). In this case we assumed that geometry and kinematic
240 characteristics that lead to define the limits between major faults in the literature act
241 as barriers for fault rupture propagation.

- 242 - Hypothesis 3 (hyp. 3): This hypothesis allows linked ruptures between selected major
243 faults with similar geometries and kinematics, while these are excluded between faults
244 with less similarities on these parameters. This leads to the definition of three sub-
245 systems, within which multi-fault ruptures are allowed, but not between them (Fig.
246 2a). We propose a CF-PF sub-system, a LTF-CAF-BSF sub-system and an AMF sub-
247 system. The first one is characterized by vertical dipping left-lateral strike-slip faults
248 (Table 1). The second one is formed by predominantly high angle S-SE dipping faults
249 with mainly reverse components (CAF and BSF). LTF, although being classified as
250 mainly strike-slip, it has been considered within this sub-system because it limits the
251 southern part of the mountain range uplifted by CAF suggesting its relationship with
252 this fault. In addition, ongoing research in the area identified fault branches related to
253 LTF with strong reverse components. The third sub-system is formed by AMF, a
254 strike slip NW dipping fault.
- 255 - Hypothesis 4 (hyp. 4): No restrictions were made in this hypothesis from CF to BSF
256 (Fig. 2a). We considered that given a particular event, a rupture could propagate
257 across both systems. On the other hand and as for hyp. 3, AMF is considered apart
258 due to its contrastingly opposite sense of dip compared to the rest of the faults.

259 **3.2. Geological fault parameters as inputs for the calculations**

260 A current challenge in the EBSZ is the difficulty to have a complete and reliable dataset
261 of fault geological parameters for all its major faults, such as slip rates and rates of large
262 earthquakes. Most paleoseismological studies have typically focused on specific branches
263 of major faults while some of the faults remain poorly studied to date. This causes
264 heterogeneity on how the knowledge on faults is distributed. Accordingly, constraining
265 the geological parameters for some of the faults considered is a difficult task and, for our

266 modelling purposes, it required taking a number of assumptions and extrapolating data
267 among different fault sections (see Appendix).

268 For this reason, we emphasized the revision of the slip rates on the EBSZ faults after
269 discussion in the frame of the Fault2SHA-Betics working group at the Eastern Betics
270 (García-Mayordomo et al., 2018), focusing on the less studied structures.

271 3.2.1. Slip rates

272 The slip rates and uncertainties of the faults were directly obtained from published
273 geological and paleoseismological studies, although the methods to infer them vary
274 between studies (Table 1 and Appendix). Slip rate data are inferred mainly from the
275 displacement of geological markers, but for different time periods depending on the fault.
276 CF has additional slip rates coming from geodetic measures consistent with geological
277 estimations (Table 1).

278 Geological slip rates on faults have been assumed to be seismic slip rates in this study.
279 We are aware that part of the slip rates considered may result partially from aseismic slip
280 and it is one of the uncertainties. However, we do not think that the contribution of the
281 aseismic slip in the EBSZ faults is that relevant because: i) Creeping is usually associated
282 with high levels of microseismicity (Malservisi et al., 2005; Scholz, 1990), which are not
283 found at the EBSZ. ii) Creep tends to be highly localized at the surface and creeping faults
284 tend to lack large brittle-deformation structures and lack deposits resulting from
285 coseismic movements (colluvial wedges, etc.) (McCalpin, 1996). Contrarily, the EBSZ
286 faults show many evidences of brittle deformation that splay upwards to the free surface,
287 indicating rapid deformation (e.g. as seen in trenches by Ferrater, 2016; Martín-Banda et
288 al., 2015; Martínez-Díaz et al., 2018). iii) There is no evidence of historical offsets, even
289 small, in anthropic structures (walls, roads, etc.) that may be hundreds of years old and

290 cross the traces of the faster faults (i.e. AMF, CF). They should be displaced if creep was
291 dominant or even half of the total slip rate.

292 Stich et al. (2007) suggest that only ~24% of the total slip rate in the Betic-Alboran-Rif
293 area is explained by the instrumental catalogue seismicity over a 21 year period, and that
294 the remaining 76% might be generated in either aseismic processes or be accumulating
295 as elastic deformation, but there is no way to distinguish among these two processes. We
296 think that an important part of that 76% might be released as large seismic events,
297 considering that the EBSZ is a low-strain region and that the last large events are previous
298 to the 20th century (e.g. 1829 Torrevieja and 1674 Lorca earthquakes). Paleoseismic
299 results in the area evidence that faults have much larger recurrence intervals than the time
300 window of the seismic catalogue.

301 As it can be seen in figure 2b and table 1, slip rate values are remarkably different from
302 one source to another. The faults that have higher slip rate values are those that have been
303 object of most paleoseismological, geomorphological and geodetic studies during the last
304 decades (i.e. AMF-1 and 2, CF) and thus have better constrained geological parameters
305 with lower uncertainty intervals. Conversely, faults that have been object of very few or
306 no paleoseismological and geodetic studies have systematically lower estimated slip rate
307 values. This has to do with the fact that their slip rates are mainly based on the long-term
308 uplift of mountain fronts and sedimentary units (i.e. PF-1 and 2, BSF-1 to 3, CAF-2,
309 AMF-4). As a result, the net slip rate is inferred from the vertical slip rate (Table 1), which
310 carries large uncertainties. The time frame of this data is much longer than for the other
311 faults and the kinematics of some sections are not clear.

312 Due to lack of data, for the cases of PF-3, CAF-2, BSF-4 and AMF-3, slip rate values
313 were established following a number of geological expert criteria explained in the

314 Appendix. The details and the type of geological information used by each study to infer
315 the slip rate of each individual fault are also explained there.

316 3.2.2. Paleorates

317 Annual rates of large earthquakes or paleoearthquakes (paleorates) were inferred from
318 minimum and maximum recurrence intervals published in the available paleoseismic
319 literature from trench data. Mean values have been calculated for each different
320 recurrence distribution (Table 2). The methods used to infer such paleorates in each
321 published study are indicated in table 2 and detailed in the Appendix. These data are
322 considered when comparing the SHERIFS models with the geological information in the
323 discussions.

324 For all cases, the magnitude of the paleorates for all faults was assumed to be a minimum
325 of $M_w 6.25 \pm 0.25$. This threshold was selected because statistically, earthquakes of $M_w <$
326 6.0 are less than 50% likely to rupture the surface (Biasi and Weldon, 2006) and hence to
327 be recorded as fault ruptures in the paleoseismic record. Data by Bonilla (1982),
328 McCalpin (1996) or the Unified Database of Surface Ruptures (SURE; Baize et al., 2019)
329 support this selection. Additionally, very shallow earthquakes at the EBSZ such as the
330 $M_w 5.1 \pm 0.1$ 2011 Lorca earthquake (IGN-UPM working group, 2013) have not ruptured
331 the surface, and events identified in trenches, despite the uncertainties of these
332 estimations, infer slips per event consistent with $M_w > 6.0$ (e.g. Ferrater, 2016; Moreno,
333 2011).

334 3.2.3. Other parameters

335 Geological parameters of the faults such as dip, kinematics, fault traces, length and
336 seismogenic depth were extracted from the Quaternary Active Faults of Iberia database
337 (QAFI) (García-Mayordomo et al., 2017, 2012; IGME, 2015a), which compiles the data

338 on the literature from each fault. Exceptionally, for PF we used the kinematics proposed
339 by Roquero et al. (2019), since it is more recent (Table 1). However, García-Mayordomo
340 (2005), as compiled in the QAFI database, considers PF as a dip slip fault and the net slip
341 rate estimations are inferred from this consideration. Hence, it is important to recognize
342 that the net slip rate for this fault is a minimum and it is subject to large uncertainty as it
343 strongly depends on its kinematics, which is still not clear. Although these discrepancies,
344 our modelling does not rely on the kinematics of the fault since the scaling law used is
345 valid for all types (see section 3.3.1).

Geological fault parameters used for the modelisation										
Fault name	Fault section ID	Dip (°)	Main kinematics	Seismogenic depth (km)		Fault length (km)	Net slip rate (mm·yr ⁻¹)			Type of information used to infer slip rate (references) and time frame covered
				Upper	Lower		Min.	Mean	Max.	
Carboneras fault (CF)	CF-1	90	Strike-slip	0	11.0	39.1	1.1	1.2	1.3	Displaced onshore fluvial/submarine channels, trench offsets in fluvial channels and GPS data (Echeverria et al., 2015; Moreno, 2011); since Pliocene - Holocene.
	CF-2	90	Strike-slip	0	11.0	59.6	1.1	1.2	1.3	
	CF-3	90	Strike-slip	0	11.0	39.5	1.1	1.2	1.3	
Palomares fault (PF)	PF-1	90	Strike-slip	0	8.0	41.1	0.01	0.04	0.08	Tectonic uplift of terraces and alluvial fans (García-Mayordomo, 2005 and references); since lower-middle Pleistocene.
	PF-2	90	Strike-slip	0	8.0	18.5	0.01	0.04	0.08	
	PF-3	90	Strike-slip	0	8.0	21.1	0.04	0.1	0.16	Analogy with LTF and PF-2 (expert opinion; see Appendix).
Los Tollos fault (LTF)	LTF	85	Strike-slip	0	8.0	16.0	0.06	0.16	0.25	Recurrence intervals in paleoseismological trenches (Insua-Arévalo et al., 2015); since 12 kyr.
Carrascoy fault (CAF)	CAF-1	70	Reverse	0	12.0	18.2	0.29	0.37	0.45	Restoration of deformed units, consistent with offsets in trenches (Martín-Banda et al., 2015); since 209.1 kyr.
	CAF-2	85	Strike-slip	0	12.0	13.1	0.48	0.53	0.58	Tectonic uplift of sedimentary units (based on unpublished research; see Appendix); since 160 kyr.
Bajo Segura fault (BSF)	BSF-1	60	Reverse	1.0	12.0	11.6	0.25	0.33	0.41	Tectonic uplift of continental units (Alfaro et al., 2012a) ; since 2-3 kyr.
	BSF-2	60	Reverse	1.0	12.0	9.2	0.25	0.33	0.41	
	BSF-3	60	Reverse	1.0	12.0	7.7	0.12	0.2	0.3	Assigned by analogy to BSF-3 section (expert opinion; see Appendix). Consistent with new GPS results (Borque et al., 2019).
	BSF-4	60	Reverse	1.0	12.0	29.3	0.12	0.2	0.3	
Alhama de Murcia fault (AMF)	AMF-1	70	Strike-slip	0	12.0	34.1	1.6	1.65	1.7	Displaced fluvial channels (Ferrater, 2016; Ferrater et al., 2017); since 200 kyr for AMF-1, 30 kyr for AMF-2.
	AMF-2	70	Strike-slip	0	12.0	19.7	0.8	1.0	1.2	
	AMF-3	70	Strike-slip	0	12.0	11.3	0.01	0.07	0.1	Based on expert opinion from the QAFI database (see Appendix).
	AMF-4	45	Strike-slip	0	12.0	23.9	0.07	0.2	0.37	Tectonic uplift of sedimentary units (Herrero-Barbero, 2016); since late Miocene- Pliocene.

346 Table 1. Faults data used for the MFD calculation with the SHERIFS code. Slip rate data was extracted from the main studies on the faults. The
 347 type of information from where slip rates have been inferred in their respective references are indicated, although more details are explained in the
 348 Appendix of this paper. Fault sections ID are mapped in figure 2a.

Paleoearthquake rate estimations							
Studies	Recurrence interval (kyr)		Cumulative paleoearthquake rate (eq/yr)			Fault section ID	Type of information used to infer recurrence
	Min.	Max.	Min.	Mean	Max.		
Ferrater (2016)	2.0	5.3	1.89E-04	3.44E-04	5.00E-04	AMF-2	Age constraints of paleoevents in trenches.
Insua-Arévalo et al. (2015)	2.2	6.86	1.46E-04	2.44E-04	4.55E-04	LTF	
Martín-Banda et al. (2015)	2.6	4.0	2.50E-04	3.08E-04	3.85E-04	CAF-1	
Moreno (2011)	1.15	13.8	7.25E-05	1.96E-04	8.70E-04	CF-3	
Ortuño et al. (2012)	15.0	29.0	3.45E-05	4.71E-05	6.67E-05	AMF-1	
Martínez-Díaz et al. (2018)	0.34	3.12	3.21E-04	7.97E-04	2.96E-03	AMF-1	Maximum magnitude model

349 Table 2. Recurrence intervals extracted from the paleoseismological studies and
350 cumulative annual rates of paleoearthquakes ($M_w \geq 6.25 \pm 0.25$) inferred from these
351 studies. The types of information used for the calculation of the recurrence values in each
352 study are indicated (see the Appendix for details) as well as the fault sections where these
353 studies developed; see figure 4 for map location. Values are rounded to two decimal
354 digits.

355 3.3. SHERIFS method

356 The flexibility of the SHERIFS methodology makes it well suited for regions where
357 seismic and geodetic data are insufficient to characterize the activity of faults and hence
358 geological data is the prime source of information on fault characteristics, long-term
359 behavior and seismic potential, as it is the case of the EBSZ.

360 SHERIFS treats the slip rate of each individual fault of the system as a budget, which is
361 consumed by the iterative steps of the method and converted into rates of earthquakes
362 assuming a given shape of a target MFD set at the fault system level. Iteratively,
363 SHERIFS picks a magnitude according to the target MFD and picks a rupture whose size
364 corresponds to this magnitude. An increment of the slip-rate budget of the faults involved
365 in this rupture is converted into earthquake rate. The iterative process goes on until the

366 slip-rate budget of limiting faults is exhausted. See Chartier et al. (2019) for details on
367 SHERIFS iterative process and how the target MFD is set.

368 In some cases, in order to fit the target MFD, not all the slip rate can be converted into
369 seismic moment rate and the remaining slip rate budget (called Non-Main-Shock slip or
370 NMS) can be considered as either post-seismic re-adjustments or creep, or a modelling
371 error. This NMS has important implications in the models; a high NMS proportion is
372 likely a suggesting a modelling error due to an incompatibility between data, target MFD
373 and rupture hypotheses. For example, the slip-rate value of some fault cannot be
374 converted into seismicity rates with a given set of rupture hypotheses while respecting
375 the target MFD shape. However, a NMS value different than zero is not necessarily a
376 modelling incompatibility and can reflect the possibility for some faults to spend a non-
377 negligible amount of their slip-rate as non-seismic processes such a post-seismic creep.

378 The required geological inputs of the SHERIFS method are: i) a 3D geometry of the fault
379 system, ii) a list of potential fault sources (i.e. individual fault sections) and iii) the slip
380 rate range of each individual fault. Additionally, the calculation process requires to set up
381 iv) a specified target shape for the MFD of the fault system (e.g. the b value of a
382 Gutenberg-Richter), v) a scaling relationship to estimate the magnitude of ruptures, vi)
383 the minimum magnitude of earthquakes produced by the faults that would be of interest
384 for the seismic hazard assessment and vii) different hypotheses/scenarios of fault and
385 multi-fault ruptures.

386 The method allows to explore the epistemic uncertainties of the parameters involved in
387 the calculations (e.g., fault slip rate, maximum magnitude of rupture, b-value of the MFD
388 target shape, etc.) by sampling them randomly in order to produce n (n=20 in our study)
389 models of annual earthquake rates for each multi-fault rupture hypothesis considered.

390 Finally, each modelled MFD of each rupture hypothesis is compared to the seismicity
391 rates from the regional catalogue and the paleorates deduced from paleoseismological
392 studies (Figs. 3 and 4). Furthermore, based on the outcome of this check, SHERIFS allows
393 to incorporate a weight to each resulting model; we suggest weighting the four multi-fault
394 rupture scenarios in order to consider their epistemic uncertainty in a logic tree for future
395 PSHA calculations.

396 3.3.1. Model parameters

397 Wells and Coppersmith (1994) for rupture area and ‘all type of kinematics’ was used to
398 calculate the M_{\max} . A shear modulus of 30 GPa was assumed representative for the
399 calculation of seismic moment in the area. For the computation of each MFD, twenty
400 random samples of the slip rate on faults, the b-value and M_{\max} were explored. Minimum
401 magnitude (M_{\min}) was set at M_w 4.0, since below that magnitude earthquakes are not
402 likely to be damaging and therefore not of interest for a hazard model. We assume all the
403 seismicity over M_w 4.0 within the buffer area defined in fig. 1b to be related to the studied
404 fault system, because it is a narrow area (~30 km wide; Fig. 1b) constrained to the surface
405 projection of the major faults of the EBSZ. In this sense, Stich et al. (2010) obtain moment
406 tensors calculated on the Betic-Alboran shear zone for the 2005-2008 period (all $M_w <$
407 5.0 at the EBSZ) that are compatible with the main kinematics of the EBSZ major faults.
408 Out of this period, other $M_w <$ 5.0 earthquakes show compatible moment tensors and are
409 also related to these faults, as highlighted by Martínez-Díaz et al. (2012b) for AMF (e.g.
410 1977 M_w 4.2, 2000 M_w 3.7, 2000 M_w 3.8 and 2011 M_w 4.8 Lorca earthquakes). Despite
411 this, we are aware of the possible limitations of assuming all seismicity happening on the
412 known faults, because earthquakes, especially lower magnitudes, may occur out of their
413 extent (Fig. 1b). However, it is important to consider that a big part of the catalogue for

414 $M_w \geq 4.0$ at the EBSZ is pre-instrumental and historical, which implies that the location
415 of epicenters is subject to significant uncertainty.

416 The earthquake catalogue used to check the synthetic MFDs is the one used in the frame
417 of the update of the Spanish national seismic hazard map (see details in IGN-UPM
418 working group, 2013), but without de-clustering and clearing of foreshocks and
419 aftershocks. Moment rate budgets used in SHERIFS are based on geological slip rates,
420 which in fact, integrate the main shocks as well as foreshocks, aftershocks, clusters
421 aseismic slip, etc. The resulting catalogue includes 2839 earthquakes of $M_w \geq 4.0$ from
422 year 1048 AD to June 2011. In the EBSZ, the maximum magnitude (M_{max}) corresponds
423 to the $M_w 6.6 \pm 0.2$, 1829 Torrevieja earthquake, however, larger earthquakes could have
424 happened given the large uncertainties in magnitude estimation of some historical
425 earthquakes. For example, the 1518 Vera earthquake has an estimated magnitude of M_w
426 6.2 ± 0.8 , meaning that the event could have reached magnitudes up to $M_w 7.0$ with a
427 34.1% of probability. The completeness years of the catalogue are shown in table 3.

Earthquake catalogue	
Magnitude range	Year of completeness
3.0-3.4	1978
3.5-3.9	1975
4.0-4.4	1908
4.5-4.9	1883
5.0-5.4	1800
5.5-5.9	1520
≥ 6.0	1048

428 Table 3. Completeness years of the earthquake catalogue in SE Spain (IGN-UPM
429 working group, 2013).

430 In order to better compare the MFDs of each scenario, only catalogue earthquakes
431 occurring within the seismogenic crust of the EBSZ were considered, which is assumed
432 to have thicknesses ranging from 8 to 12 km depending on the area (García-Mayordomo,

433 2005; Table 1). This tried to ensure that earthquakes located in this depth range were more
434 likely produced by the faults in our study and not by deeper unidentified sources.

435 The buffer area used to extract the seismicity (Fig. 1b) was originally defined as an area
436 source for the calculation of the Spanish seismic hazard map and was delineated based
437 on the surface projection of the faults (IGME, 2015b; IGN-UPM working group, 2013).
438 We considered an MFD target shape that follows a Gutenberg-Richter distribution (GR;
439 Gutenberg and Richter, 1944) with a b-value in the range of 0.8-1.2, whose central value
440 is coincident with the b-value of 1.03 assigned to the EBSZ (IGME, 2015b; IGN-UPM
441 working group, 2013). This wide b-value range was explored in order to prevent the
442 resulting MFDs of our hypotheses from being limited or biased by such value or imposed
443 shape of the MFD.

444 See the datasets available on the Mendeley Data of this paper (Gómez-Novell et al., 2019)
445 for more details on the SHERIFS parameters and models performed in this study, the raw
446 inputs and output files of the calculations, including the fault parameters and the seismic
447 catalogue used.

448 **4. Results**

449 **4.1. Modelled earthquake rates from SHERIFS**

450 The modelling with SHERIFS provided four MFDs for each rupture hypothesis set which
451 refer to the whole EBSZ system (Fig. 3). Each of the four obtained GR MFDs is composed
452 by a set of twenty samples per 0.1 magnitude increment, which form twenty different
453 MFDs. These twenty distributions that result from the random sampling process of the
454 input data (slip rate, M_{\max} and b-value) compose the overall curve of each hypothesis.

455 As figure 3 illustrates, the hypotheses that consider larger multi-fault rupture scenarios
456 show larger M_{\max} . Annual rate values are similar for hyp. 1 to 3 in the range of M_w 4.0-
457 6.5, while hyp. 4 shows much lower values for the whole log-linear distribution.

458 4.1.1. Performance of SHERIFS models

459 We analyze the performance of the different hypotheses in terms of the % of Non-Main-
460 Shock slip (NMS). Its relation to the seismic moment rate describes the performance of
461 the hypotheses in SHERIFS. From hyp. 1 to 3, more than 70% of the slip rate is converted
462 into seismic moment rate, and thus only 30% of the slip is assumed as NMS for most of
463 the samples on the slip rate and M_{\max} (Fig. 3). On the other hand, in hyp. 4, only 10% of
464 the slip rate (i.e. 90 % of NMS) is converted into seismic moment rate and hence it does
465 not perform as well as the other hypotheses.

466 We explain the %NMS in our models as a consequence of the configuration of ruptures
467 of each hypothesis in relation to the slip rate variations between fault sections. This
468 configuration affects how the slip rate budget is consumed in the different iterations of
469 the modelling.

470 The fact that large multi-fault ruptures involve slower sources, causes their slip rate
471 budget to be rapidly exhausted in the highest magnitude ruptures, since they are the ones
472 that consume most seismic moment rate. When this happens, the target MFD of the
473 system is set and the rest of the calculation follows this imposed shape. In the case of the
474 EBSZ, the rates of very large ruptures (i.e. hyp. 4) are significantly low because they are
475 limited by slow moving faults (e.g. PF, LTF, CAF, BSF; Fig. 2b, table 1). When the target
476 is set in the high magnitudes, the rates of the whole distribution are therefore lowered.
477 Consequently, for such large rupture scenarios the system has a lot of remaining slip rate
478 budget not converted into seismic moment (i.e. NMS). This NMS is hosted by the faster

479 faults, which are the ones whose budget is not exhausted. Such effect also evidences the
480 fact that the poor knowledge on the slip rate for some of the faults, i.e. the ones with lower
481 slip rates, especially PF (Table 1), limit the way the models consume their budget and the
482 resulting MFDs. Thus, it is critical to constrain them in future paleoseismic studies.

483 Because NMS cannot be directly interpreted as a nature-related effect, but as an artefact
484 of the model linked to the rupture hypotheses, MFD target and input data set, we use it to
485 evaluate the adequacy of our hypotheses. In the line of Chartier et al. (2019), we have set
486 a threshold of 30% NMS for the overall system as an indicator of models that are not
487 sufficiently satisfactory. This value is in agreement with studies that estimate that post-
488 seismic moment release reaches at most 30% of the total moment released in seismic
489 events. The normal faulting M_w 5.9, 1999 Athens earthquake, for instance, was
490 interpreted to have released aseismically 30% of the total moment (Baumont et al., 2004).
491 The strike-slip faulting M_w 5.6 1979 Homestead and the M_w 7.5 1992 Landers
492 earthquakes in California showed estimated post-seismic releases of about 10-15% (Shen
493 et al., 1994; Stein and Lisowski, 1983, respectively).

494 Hypotheses 1 to 3 have 80-90 to 100% of their samples below 30% of NMS (Fig. 3),
495 hence it could be interpreted as part of the slip rate that is not consumed seismically.
496 Conversely, the high %NMS of hypothesis 4 suggests that the fault rupture configuration
497 is not adequate given the methodology and fault input data and hence, a modelling error
498 is detected. This is also evidenced by the high dispersion of the log-linear GR curve of
499 this model compared to the others.

500 **4.2. Comparison with the earthquake catalogue and paleoseismic data**

501 4.2.1. Seismicity rates from the earthquake catalogue

502 We visually analyzed the fit between the SHERIFS MFDs and the annual seismicity rates
503 obtained from the regional earthquake catalogue (IGN-UPM working group, 2013). Note
504 that the GR curve from the catalogue covers a dispersed range of annual rates due to the
505 exploration of the code within the magnitude uncertainty of the events in the catalogue
506 (Fig. 3). The dispersion is higher for the high magnitudes ($M_w \geq 6.0$) due to the large
507 uncertainties related to the magnitude estimation of large historical events at the EBSZ.
508 The MFD from hyp. 2 shows the better fit with the seismicity rates especially for M_w 4.0-
509 6.0 (Fig. 3). MFDs from hyp. 1 and 3 show similar good agreements with the catalogue
510 as well, but their fit is poorer; hyp. 1 slightly overestimates the catalogue, while hyp. 3
511 underestimates it. The curve from hyp. 4, on the other hand, shows a strong disagreement
512 with the seismic catalogue, where the rates modelled highly underestimate the seismicity
513 rates (Fig. 3).

514 4.2.2. Paleorates

515 Annual earthquake rates from paleoseismological research at the EBSZ (see table 2) were
516 compared with the modelled curves for the $M_w \geq 6.0$ range. (Fig. 4). The paleorates from
517 each paleoseismological study (Table 2) are plotted together with the participation rates
518 of each corresponding fault section for each rupture hypothesis (Fig. 4). These GR curves
519 show the participation rates resulting from considering all the ruptures hosted in each
520 fault section per rupture scenario.

521 As it is observed from the plotted figures (Fig. 4), hyp. 4 does not match the paleorates
522 estimated from the studies at the EBSZ. Hyp. 2 and 3, on the other hand, predict better
523 the inferred paleorates for most of the faults considering their uncertainties. In most cases,
524 the differences between these two hypotheses are barely noticeable, as it is the case of the
525 paleorates of CF, AMF-2 and CAF-1, but for LTF hyp. 3 has the better fit (Fig. 4), since

526 both hyp. 1 and 2 assume the same rupture model for this fault (Fig. 2a). The participation
527 rates from hyp. 1 show, in some sites, good results with the paleorates, especially in AMF-
528 2, but not superior than hyp. 2 and 3. Note also that the paleorates of AMF-1 by Ortuño
529 et al. (2012) do not fit the modelled rates, as we discuss in section 5.1.2.

530 **5. Discussion**

531 **5.1. Analysis of the modelling results with the datasets**

532 5.1.1. Seismicity rates from the catalogue

533 The better fits of the seismic catalogue with hyp. 2 especially, but also hyp. 1 and 3 (Fig.
534 3) do not allow determining if these hypotheses describe the manner in which the EBSZ
535 system works. They only show that, given the methodology used, the input data and the
536 rupture hypotheses explored, the models are more consistent with the low-moderate
537 magnitude seismicity of the EBSZ than others. Hence, no hypothesis should be ruled out,
538 especially considering the epistemic uncertainties linked to some slip rate estimations.
539 However, the consistency of these models can be used to guide their weight in a logic tree
540 for PSHA.

541 Overestimation of the seismicity rates by hyp. 1 could be caused by two factors: i) a non-
542 adequate segmentation model for the faults that considers too short fault sections and
543 hence, higher earthquake rates than the catalogue, ii) the already acknowledged
544 uncertainties and poor reliability of some geological fault data affecting the modelisation.
545 Underestimation of the catalogue by hyp. 3 could be explained by the largest ruptures
546 allowed in this model that may slightly contribute to limit the annual rates in the lower
547 magnitudes. We are not able to distinguish the contribution of each option, but further
548 research should focus first on exploring the impact of new segmentation models and

549 second, on constraining critical fault parameters (i.e. slip rate) as is discussed in sections
550 5.1.2 and 5.2.

551 Considering the consistency of the models with the catalogue, hyp. 2 should have more
552 weight in a PSHA, followed by hyp. 1 and 3 similarly, and finally hyp. 4.

553 5.1.2. Paleorates

554 Recent studies on active faults at the EBSZ allowed to infer slip rates in specific portions
555 of such faults as well as to calculate rates of earthquakes. In this study, the rates inferred
556 from paleoseismology are a qualitative way to analyze the prediction of the models in the
557 high magnitude range, where the seismic catalogue is not well represented. Similar to the
558 case of the catalogue, the agreement or disagreement of the paleorates with the modelled
559 rates does not provide a way to accept or rule out any of our hypotheses, but to weight
560 them for future PSHA. Paleorates, though, have an additional problem related to the high
561 uncertainties and low resolution of the paleoseismological data in the study area. One of
562 these problems applies mainly to the magnitude of the events inferred from geological
563 observations.

564 We considered that all the paleorates reflect earthquakes of $M_w \geq 6.25 \pm 0.25$. However,
565 lower magnitude earthquakes can rupture the surface as well (i.e. the M_w 5.5 1975
566 Homestead Valley earthquake; Schwartz, 2018) implying that they could be observed in
567 the EBSZ trenches and incorporated to the paleorate estimations as larger. This
568 uncertainty has a difficult assessment at the EBSZ, although our magnitude threshold
569 selection is supported by statistical observations of fault ruptures (see section 3.2.2).

570 Another one affects directly the paleoearthquake rate estimations and concerns the fact
571 that paleoseismology always provides a minimum number of paleoearthquakes and
572 hence, maximum recurrence intervals. There are two main causes for this:

573 - The first is that paleoseismic studies are limited to specific regions and branches of a
574 fault and rarely account for the whole structure. Surface ruptures are usually not
575 continuous along strike and do not always accommodate ruptures on the same branch.
576 Recent examples such as the 2016 Mw 7.8 Kaikoura earthquake (New Zealand)
577 support this observation, where a significant part of the deformation was
578 accommodated off-fault (e.g. Kearsse et al., 2018). This way, the missing of events in
579 the paleoseismic record is likely and higher paleorate values should be expected.

580 Following this reasoning, our hyp. 4 is not suitable, since increased paleorates would
581 lead to even much stronger disagreement with the modelled curves of such
582 hypothesis. The strong underestimation of the paleorates by hyp. 4, together with its
583 misfit with the catalogue and high %NMS suggesting modelling issues, lead us to
584 estimate that this rupture hypothesis treats unrealistically long multi-fault rupture
585 possibilities considering the data used and the rupture hypotheses explored.

586 - The second reason is linked to the lack of depositional continuity, as highlighted by
587 Ortuño et al. (2012) in AMF-1. The discontinuous geological record hinders the
588 identification and time constraining of the number of paleoseismic events observed
589 and might lead to erroneous paleorate estimations. In figure 4, the paleorate from
590 Ortuño et al. (2012) in AMF-1 is underestimated due to this effect, resulting in a
591 misfit with the modelled MFDs of hyp. 1-3 and the paleorate by Martínez-Díaz et al.
592 (2018).

593 Hyp. 2 and hyp. 3 both fit well with the paleorates suggesting that, given the inputs and
594 rupture models explored, multi-fault rupture scenarios involving single or several whole
595 faults allow to explain the paleoearthquake rate estimations. The paleorate fits of these
596 hypotheses are consistent with their fits with the catalogue, especially hyp. 2 (Fig. 3).
597 This enhances the robustness of these models.

598 Hyp. 1 performs good predictions of the paleorates as well, especially for AMF, but the
599 fits are less consistent in general, compared to hyp. 2 and 3 (Fig. 4). It is important to
600 recall that the most suitable hypothesis should agree not only with the rates of the higher
601 magnitudes, but also with the rates of smaller magnitudes represented by the seismic
602 catalogue. Hyp. 2 and hyp. 3 satisfy this requirement more correctly than hyp. 1 (Fig. 3)
603 and accordingly should have more weight in subsequent PSHA. Similarly to the analysis
604 with the catalogue, the weaker agreement of hyp. 1 with the paleorates could mean that
605 either or both the segmentation proposed for these faults is not adequate and larger
606 ruptures should be expected (e.g. hyp. 2 and 3), and that paleoearthquake data is
607 underestimated. Both epistemic uncertainties should be explored in further research,
608 although the latter is more difficult to assess, since the issues are somehow inherent to the
609 paleoseismic approaches. More paleoseismic research might help improve and better
610 constrain paleoearthquake data at the EBSZ.

611 Finally, the method used to infer the paleorates in each study (Table 2) is conditioning
612 the robustness of the results, because it affects the independence of the analysis. Martínez-
613 Díaz et al. (2018) results are based in a single observed paleoevent in a trench. The
614 paleorates are inferred using the geological moment rate from the fault slip rate and the
615 seismic moment of the maximum expected rupture following the maximum magnitude
616 model from Wesnousky (1986). Since SHERIFS uses slip rates as inputs, the models for
617 this fault are somehow linked to the paleorates and the analysis cannot be claimed as
618 completely independent. Martín-Banda et al. (2015) infer the paleorate for CAF-1
619 similarly, but the value is consistent with the one inferred independently from age
620 constraints of paleoevents in trenches. Insua-Arévalo et al. (2015) for LTF, infer the slip
621 rate of the fault from the paleorates and the offsets in the trenches. This dependence
622 between models and data to weight them does not invalidate the analysis, though; the

623 modelled MFDs are not build relying only on the exploration of slip rates but also on fault
624 rupture scenarios (M_{max}) and the b value, which in this case are independent variables.

625 In the other faults explored, the paleorate estimations (Table 2) are inferred from dividing
626 the number of paleoevents in trenches over their observational time period, thus they are
627 not dependent on the slip rate or maximum expected rupture; they are independent data
628 to compare with the modelled earthquake rates.

629 **5.2. Additional considerations on the modelling**

630 The present study raised several critical questions concerning the databases that may be
631 of interest for other low-strain regions similar to the EBSZ and for PSHA modelers.

632 SHERIFS constitutes a useful tool to discuss the epistemic uncertainties affecting a given
633 fault system for fault source modelling in PSHA. In the particular case of the EBSZ, as
634 in most low-strain regions, the main epistemic uncertainties are related to the geological
635 fault input data used, especially affecting slip rate and paleoearthquake rate estimations,
636 and the definition of fault rupture scenarios to be explored. In this sense, the results of
637 this study, far from precisely determining the EBSZ behavior, have shown to be a
638 practical tool to highlight where these uncertainties are more important and limiting. One
639 clear example is PF, one of the less studied faults of the system with contrasting low slip
640 rates (Table 1) that affect the modelling and the resulting distribution of hyp. 4. This
641 highlights where future research should focus to better constrain these parameters and
642 which rupture models are not adequate in the calculation given the input data. Despite
643 this, geodetic data suggests that in the transect between PF and AMF (Fig. 1b), most part
644 of the slip rate is absorbed by the former (Echeverria et al., 2013), which could explain
645 the low values assigned to PF. Knowing and assessing these uncertainties is critical to
646 account for them in fault-based PSHA.

647 In addition and despite the limitations, SHERIFS is also a good tool to determine the
648 weights that different fault source models should have in PSHA according to their
649 consistency with the seismic catalogues and paleoseismic studies.

650 **5.3. Perspectives**

651 It is critical that researchers challenge classical segmentation models and consider faults
652 as systems of geological structures that can interact. This is especially relevant in regions
653 of distributed deformation along complex fault systems (e.g. Berryman et al., 2012) as it
654 could be the case of the EBSZ, where the rupture models selected may have important
655 repercussions on PSHA.

656 The research in this paper constitutes the first step for a fault-based PSHA at the EBSZ
657 in which epistemic uncertainties of the available databases are discussed. Hence, further
658 work needs to be focused towards reducing the uncertainties raised, especially from the
659 geological and paleoseismic records. Moreover, the approach might serve as an example
660 for similar seismo-tectonic contexts, as well as for defining deterministic earthquake-
661 scenarios for engineering applications.

662 In further modellings and especially for PSHA we also find necessary to consider a
663 portion of the seismicity from the catalogue as background in SHERIFS calculations.
664 Clearly, not all the seismicity within the buffer area defined is generated by the faults in
665 our models, especially smaller magnitudes (Fig. 1b). This is critical because it might
666 directly affect the seismic hazard of the region for short or mid-term return periods.

667 In the models we explored a particular GR distribution; the one used for the Spanish
668 seismic hazard map (IGN-UPM working group, 2013). Considering the data available
669 from the catalogue and paleoseismic studies, we do not have clear criteria to dismiss it.
670 However, other studies in other regions, for instance New Zealand (Stirling and

671 Gerstenberger, 2018), have proved that GR distributions do not always describe annual
672 rates of the high magnitudes derived from paleoseismic data. Exploring these options at
673 the EBSZ in further research is also important due to its repercussions on the seismic
674 hazard assessments.

675 **Conclusions**

676 In this study, we have modelled the magnitude-frequency distributions of the Eastern
677 Betics Shear Zone (SE, Spain) using selected available geological data on faults and
678 exploring four rupture hypotheses. The first hypothesis only allows ruptures within the
679 extent of the segmentation proposed in literature and the other three allow multi-fault
680 ruptures with maximum lengths that range from whole faults to nearly the whole system.
681 Each hypothesis is defined based on selected geological rules.

682 The results suggest that the occurrence of multi-fault ruptures extending longer than the
683 classic sections defined in the literature and involving individual whole faults or several
684 whole faults (hypotheses 2 and 3, respectively) are consistent with both the seismic
685 catalogue and the available paleoearthquake record. The other hypotheses, especially
686 hypothesis 4, are less consistent with these data. Despite their different performance, no
687 hypothesis can be completely ruled out because the resulting rates are dependent on the
688 reliability and multiple epistemic uncertainties affecting the geological input data as well
689 as the criteria on the definition of the hypotheses. Instead, they are weighted for further
690 PSHA studies being hypothesis 2 and 3 the ones with higher weight.

691 The comprehensive methodology followed in this work, and particularly the use of
692 SHERIFS, is revealed as a practical method for obtaining fault-system MFDs and as a
693 practical tool for highlighting limitations and epistemic uncertainties in geological and
694 paleoseismic data of the fault system to be assessed in further research. The main

695 geological uncertainties are related to poorly constrained and unreliable slip rate
696 estimations for some faults mainly due to lack of paleoseismic research. These data have
697 a high impact on the modelling, since they limit the annual rates of earthquakes for some
698 hypotheses. On the other hand, uncertainties from paleoseismic data might lead to wrong
699 estimates of the rates of paleoearthquakes. Accounting and reducing these uncertainties
700 are key issues for the improvement of fault-based PSHA.

701 Considering faults as interacting systems is an option that needs to be acknowledged when
702 modelling seismic hazard, as evidenced by the recent experience from earthquakes
703 worldwide. This means overcoming the classical sectioning models and exploring
704 different multi-fault rupture models by combining seismic and paleoseismic data.

705 **Acknowledgements**

706 This work was supported by the PREVENT project (CGL2015-66263-R), funded by the
707 Spanish Ministry of Science, Innovation and Universities. The authors want to thank the
708 anonymous reviewers and the editor for the comments and suggestions that contributed
709 to the improvement of the present manuscript, as well as the ESC Fault2SHA working
710 group members for the fruitful discussions and work sessions that enhanced the quality
711 of this study.

712 **Appendix: Information used to infer slip rate and paleorate data on each individual**
713 **fault**

714 This appendix contains details on what type of information the slip rate data and
715 paleoearthquake rates (recurrences) are based on in each published study and for each
716 fault. This follows the information highlighted in tables 1 and 2 and the fault sections in
717 figure 2a of the paper. We also put emphasis on the expert criteria followed to assign slip
718 rate values to those faults where there is no published slip rate data available.

719 **A)** Faults whose slip rate data are directly extracted from published studies.

720 - **CF:** The lateral slip rate is inferred from geomorphological analysis onshore (CF-2,
721 3) and offshore (CF-1, 2), 3D paleoseismological studies (CF-3; Moreno, 2011;
722 Moreno et al., 2015) and geodetic studies (CF-3; Echeverria et al., 2015). All three
723 methods are coincident in the predicted slip rate values ($1.2 \pm 0.1 \text{ mm}\cdot\text{yr}^{-1}$) and valid
724 since the Pliocene but also for the Holocene. Net and lateral slip rate values show
725 similar values because 1) the vertical slip rate for this fault is one to two orders of
726 magnitude lower than the lateral ($0.01\text{-}0.3 \text{ mm}\cdot\text{yr}^{-1}$; Moreno, 2011) and 2) the
727 differences in the slip rate values are within the uncertainty range. Paleorates are
728 estimated from trenching results (Masana et al., 2018; Moreno, 2011) in the northern
729 branch of the two parallel strands that compose CF-3. In these studies, 7 or more
730 paleoearthquakes since 191 kyr were identified. However, we considered the 3 last
731 earthquakes for the last 41.5 kyr (Moreno, 2011), since the earthquake rates are
732 increased for this time period.

733 - **PF-1 and 2:** The net slip rates used are the lower and upper values of the long-term
734 uplift rates of lower-middle Pleistocene terraces and alluvial fan surfaces (see
735 discussion in García-Mayordomo, 2005). This last study considers this fault as mainly
736 dip-slip, but new recent data on PF (Roquero et al., 2019) suggest strike slip

737 kinematics, which could change the net slip rate values significantly. There are no
738 published paleoseismic studies available in this fault and hence no paleorate
739 estimations to date.

740 - **LTF:** The net slip rate of this fault is inferred from recurrence estimations of at least
741 2 paleoearthquakes observed in paleoseismic trenches and respective offsets (Insua-
742 Arévalo et al., 2015). The slip rate and paleorate estimations refer to the last 12 kyr.

743 - **CAF-1:** For this fault, the net slip rate is calculated from restoration of deformation
744 of the top a distinctive sedimentary unit exposed in trenches and cropping out in the
745 mountain slope (Red Unit; Martín-Banda et al., 2015). This is a long-term slip rate
746 for the last 209.1 ± 6.2 kyr, which is the age of the Red Unit, but the slip rate value is
747 consistent with the one obtained from offsets in younger units in the trenches for the
748 last 6.9 ± 1.8 kyr (Martín-Banda et al., 2015). The paleorates from this study are
749 calculated from the slip rate and seismic moment considering the rupture of the whole
750 section. However, these paleorates are consistent with the ones estimated from two
751 paleoevents for the last 6.0 kyr.

752 - **BSF-1 to 3:** The net slip rates of the different sections of these fault sections are
753 inferred from the uplift of 2-3 kyr old continental sedimentary units (Alfaro et al.,
754 2012a). No paleoseismic trench studies are available for these faults.

755 - **AMF-1:** The lateral slip rate in this section is inferred from offsets in fluvial channels
756 summed for all the branches that the fault shows (Ferrater, 2016; Ferrater et al., 2017).
757 Vertical slip rate estimations in this section are subject to a larger uncertainty and the
758 values are about one order of magnitude lower ($0.16-0.22 \text{ mm}\cdot\text{yr}^{-1}$; Ortuño et al.,
759 2012), hence strike-slip is the predominant kinematics of the fault. The slip rate data
760 is for the last 200 kyr. Recent paleoseismological studies in this section have also
761 been able to identify paleoearthquakes in the southwestern tip (Ortuño et al., 2012)

762 and historical earthquakes in the northeastern tip (Martínez-Díaz et al., 2018). The
763 minimum paleorates inferred from paleoseismic studies in this section are for the last
764 116 kyr (Ortuño et al., 2012).

765 - **AMF-2:** The lateral slip rate ($1.0 \pm 0.2 \text{ mm}\cdot\text{yr}^{-1}$) is inferred from offsets in fluvial
766 channels for the last 30 kyr (Ferrater, 2016; Ferrater et al., 2017). Paleoseismological
767 3D trenching in this section inferred net slip rate values in the same range (0.9 ± 0.1
768 $\text{mm}\cdot\text{yr}^{-1}$ for the last 20 kyr; Ferrater, 2016), hence vertical slip rate is negligible ($0.1 \pm$
769 $0.0 \text{ mm}\cdot\text{yr}^{-1}$). Paleoseismological studies in this section identified a minimum of 10
770 paleoearthquakes for the last 59 kyr, which allowed to infer the respective paleorates.

771 - **AMF-4:** The net slip rate in this section is estimated from long term (since late
772 Miocene-Pliocene) uplift through geological structural analysis in the mountain
773 ranges limited by this section. These methods imply large uncertainties for the slip
774 rate estimation, because factors such as sediment compaction need to be considered.
775 Although the latest studies in this section infer better constrained values ($0.13\text{-}0.18$
776 $\text{mm}\cdot\text{yr}^{-1}$; Herrero-Barbero et al., 2017) we used the wider range estimated in Herrero-
777 Barbero (2016) ($0.07\text{-}0.37 \text{ mm}\cdot\text{yr}^{-1}$) to ensure a conservative margin of uncertainty.

778 **B)** Faults whose slip rate data is inferred following expert criteria or unpublished work.

779 - **PF-3:** Slip rate estimations for this fault section are not available, since there is no
780 studies in this area. According to the values assigned, the slip rate increases from PF-
781 1 and 2 to LTF. Thus, it is feasible that, in order to accommodate this difference, PF-
782 3 has an intermediate slip rate. For this reason, we assigned to PF-3 a slip rate which
783 is the mean between the values of PF-2 and LTF. The uncertainty range assigned is an
784 intermediate value between the uncertainties of these two faults (Table 1).

785 - **CAF-2:** For this fault section there is a published net slip rate value of $0.54 \text{ mm}\cdot\text{yr}^{-1}$
786 (García-Mayordomo, 2005 and references), based on geomorphological offsets and

787 tectonic uplift (at minimum since the last 160 kyr). However, ongoing research on this
788 fault (Martín-Banda, personal communication) yields new slip rate values: 0.48-0.54
789 mm·yr⁻¹.

790 - **BSF-4:** This section of BSF is offshore and only a few studies have focused on that
791 part of the fault, hence not enough data is available to do estimations of the slip rate of
792 this section. Although some authors (e.g. Alfaro et al., 2012a) suggest that the
793 deformation associated to the BSF decreases towards the E, from a conservative
794 perspective we assigned the same slip rate range as for BSF-3 (0.12-0.3 mm·yr⁻¹),
795 which is consistent with new GPS results in that sector (Borque et al., 2019).

796 - **AMF-3:** There are no slip rate estimations for this section. In fact, the
797 geomorphological expression of this fault is scarce and hence its slip rate is probably
798 much lower than the other sections. Since it is our only source of information, we used
799 the net slip rate estimated in the QAFI database (0.042-0.097 mm·yr⁻¹) for AMF-3,
800 rounded the upper uncertainty value and enlarged considerably the lower bound
801 uncertainty, obtaining a net slip rate range of 0.01-0.1 mm·yr⁻¹. From our perspective,
802 enlarging the uncertainties accounts for a more conservative way to express the lack
803 of knowledge of this fault.

804 **References**

- 805 1. Alfaro, P., Bartolomé, R., Borque, M.J., Estévez, A., García-Mayordomo, J., García-
806 Tortosa, F.J., Gil, A.J., Gràcia, E., Lo Iacono, C., Perea, H., 2012a. The Bajo Segura Fault
807 Zone: Active blind thrusting in the Eastern Betic Cordillera (SE Spain). *Journal of Iberian*
808 *Geology* 38. https://doi.org/10.5209/rev_JIGE.2012.v38.n1.39217
- 809 2. Alfaro, P., Delgado, J., García-Tortosa, F.J., Lenti, L., López, J.A., López-Casado, C.,
810 Martino, S., 2012b. Widespread landslides induced by the Mw 5.1 earthquake of 11 May
811 2011 in Lorca, SE Spain. *Engineering Geology* 137–138, 40–52.

- 812 <https://doi.org/10.1016/j.enggeo.2012.04.002>
- 813 3. Argus, D.F., Gordon, R.G., DeMets, C., 2011. Geologically current motion of 56 plates
814 relative to the no - net - rotation reference frame. *Geochemistry, Geophysics, Geosystems*
815 12, 1–13. <https://doi.org/10.1029/2011GC003751>
- 816 4. Baize, S., Nurminen, F., Sarmiento, A., Dawson, T., Takao, M., Scotti, O., Azuma, T.,
817 Boncio, P., Champenois, J., Cinti, F.R., Civico, R., Costa, C., Guerrieri, L., Marti, E.,
818 McCalpin, J., Okumura, K., Villamor, P., 2019. A Worldwide and Unified Database of
819 Surface Ruptures (SURE) for Fault Displacement Hazard Analyses. *Seismological*
820 *Research Letters*. <https://doi.org/10.1785/0220190144>
- 821 5. Baumont, D., Scotti, O., Courboux, F., Melis, N., 2004. Complex kinematic rupture of
822 the Mw 5.9, 1999 Athens earthquake as revealed by the joint inversion of regional
823 seismological and SAR data. *Geophysical Journal International* 158, 1078–1087.
824 <https://doi.org/10.1111/j.1365-246X.2004.02374.x>
- 825 6. Bayrak, Y., Öztürk, S., Çınar, H., Kalafat, D., Tsapanos, T.M., Koravos, G.C., Leventakis,
826 G.A., 2009. Estimating earthquake hazard parameters from instrumental data for different
827 regions in and around Turkey. *Engineering Geology* 105, 200–210.
828 <https://doi.org/10.1016/j.enggeo.2009.02.004>
- 829 7. Berryman, K.R., Cochran, U.A., Clark, K.J., Biasi, G.P., Langridge, R.M., Villamor, P.,
830 2012. Major Earthquakes Occur Regularly on an Isolated Plate Boundary Fault. *Science*
831 336, 1690 LP – 1693. <https://doi.org/10.1126/science.1218959>
- 832 8. Biasi, G.P., Weldon, R.J., 2006. Estimating surface rupture length and magnitude of
833 paleoearthquakes from point measurements of rupture displacement. *Bulletin of the*
834 *Seismological Society of America* 96, 1612–1623. <https://doi.org/10.1785/0120040172>
- 835 9. Boncio, P., Lavecchia, G., Pace, B., 2004. Defining a model of 3D seismogenic sources for
836 Seismic Hazard Assessment applications: The case of central Apennines (Italy). *Journal of*
837 *Seismology* 8, 407–425. <https://doi.org/10.1023/B:JOSE.0000038449.78801.05>
- 838 10. Bonilla, M.G., 1982. Evaluation of Potential Surface Faulting and Other Tectonic
839 Deformation. USGS Open-File Report 82-732.

- 840 11. Borque, M.J., Sánchez-Alzola, A., Martín-Rojas, I., Alfaro, P., Molina, S., Rosa-Cintas, S.,
841 Rodríguez-Caderot, G., de Lacy, C., Avilés, M., Herrera-Olmo, A., García-Tortosa, F.J.,
842 Estévez, A., Gil, A.J., 2019. How Much Nubia-Eurasia Convergence Is Accommodated by
843 the NE End of the Eastern Betic Shear Zone (SE Spain)? Constraints From GPS Velocities.
844 *Tectonics* 38, 1824–1839. <https://doi.org/10.1029/2018TC004970>
- 845 12. Bousquet, J.C., 1979. Quaternary Strike-Slip Faults in Southeastern Spain. *Developments*
846 *in Geotectonics* 13, 277–286. <https://doi.org/10.1016/B978-0-444-41783-1.50044-1>
- 847 13. Chartier, T., Scotti, O., Lyon-Caen, H., Boiselet, A., 2017. Methodology for earthquake
848 rupture rate estimates of fault networks: Example for the western Corinth rift, Greece.
849 *Natural Hazards and Earth System Sciences* 17, 1857–1869. [https://doi.org/10.5194/nhess-](https://doi.org/10.5194/nhess-17-1857-2017)
850 [17-1857-2017](https://doi.org/10.5194/nhess-17-1857-2017)
- 851 14. Chartier, T., Scotti, O., Lyon-Caen, H., 2019. SHERIFS: Open-Source Code for
852 Computing Earthquake Rates in Fault Systems and Constructing Hazard Models.
853 *Seismological Research Letters*. <https://doi.org/10.1785/0220180332>
- 854 15. Cornell, C.A., 1968. Engineering seismic risk analysis. *Bulletin of the Seismological*
855 *Society of America* 58, 1583–1606.
- 856 16. De Larouzière, F.D., Bolze, J., Bordet, P., Hernandez, J., Montecat, C., Ott d'Estevou, P.,
857 1988. The Betic segment of the lithospheric Trans-Alboran shear zone during the Late
858 Miocene. *Tectonophysics* 152, 41–52. [https://doi.org/10.1016/0040-1951\(88\)90028-5](https://doi.org/10.1016/0040-1951(88)90028-5)
- 859 17. Delgado, J., Peláez, J.A., Tomás, R., García-Tortosa, F.J., Alfaro, P., López Casado, C.,
860 2011. Seismically-induced landslides in the Betic Cordillera (S Spain). *Soil Dynamics and*
861 *Earthquake Engineering* 31, 1203–1211. <https://doi.org/10.1016/j.soildyn.2011.04.008>
- 862 18. Demets, C., Gordon, R.G., Argus, D.F., 2010. Geologically current plate motions.
863 *Geophysical Journal International* 181, 1–80. [https://doi.org/10.1111/j.1365-](https://doi.org/10.1111/j.1365-246X.2009.04491.x)
864 [246X.2009.04491.x](https://doi.org/10.1111/j.1365-246X.2009.04491.x)
- 865 19. Echeverria, A., Khazaradze, G., Asensio, E., Gárate, J., Dávila, J.M., Suriñach, E., 2013.
866 Crustal deformation in eastern Betics from CuaTeNeo GPS network. *Tectonophysics* 608,
867 600–612. <https://doi.org/10.1016/j.tecto.2013.08.020>

- 868 20. Echeverria, A., Khazaradze, G., Asensio, E., Masana, E., 2015. Geodetic evidence for
869 continuing tectonic activity of the Carboneras fault (SE Spain). *Tectonophysics* 663, 302–
870 309. <https://doi.org/10.1016/J.TECTO.2015.08.009>
- 871 21. Ferrater, M., 2016. Velocitat de desplaçament de la falla d'Alhama de Murcia (Bètiques
872 Orientals); implicacions en el seu potencial sísmic. PhD thesis, Universitat de Barcelona,
873 Barcelona, Spain.
- 874 22. Ferrater, M., Ortuño, M., Masana, E., Martínez-Díaz, J.J., Pallàs, R., Perea, H., Baize, S.,
875 García-Meléndez, E., Echeverria, A., Rockwell, T., Sharp, W.D., Arrowsmith, R., 2017.
876 Lateral slip rate of Alhama de Murcia fault (SE Iberian Peninsula) based on a
877 morphotectonic analysis: Comparison with paleoseismological data. *Quaternary*
878 *International* 451, 87–100. <https://doi.org/10.1016/j.quaint.2017.02.018>
- 879 23. Field, E., Biasi, G.P., Bird, P., Dawson, T.E., Felzer, K.R., Jackson, D.D., Johnson, K.M.,
880 Jordan, T.H., Madden, C., Michael, A.J., Milner, K., Page, M.T., Parsons, T., Powers,
881 P.M., Shaw, B.E., Thatcher, W.R., Weldon, R.J., Zeng, Y., 2014. The Uniform California
882 Earthquake Rupture Forecast, Version 3 (UCERF3). *Bulletin of the Seismological Society*
883 *of America* 3, 1122–1180. <https://doi.org/10.3133/ofr20131165>
- 884 24. Frankel, A., 1995. Mapping Seismic Hazard in the Central and Eastern United States.
885 *Seismological Research Letters* 66, 8–21. <https://doi.org/10.1785/gssrl.66.4.8>
- 886 25. García-Mayordomo, J., 2015. Creación de un modelo de zonas sismogénicas para el
887 cálculo del mapa de peligrosidad sísmica de España. Madrid.
- 888 26. García-Mayordomo, J., 2005. Caracterización y análisis de la peligrosidad sísmica en el
889 sureste de España. PhD thesis, Universidad Complutense de Madrid, Madrid, Spain.
- 890 27. García-Mayordomo, J., Gaspar-Escribano, J.M., Benito, B., 2007. Seismic hazard
891 assessment of the Province of Murcia (SE Spain): Analysis of source contribution to
892 hazard. *Journal of Seismology* 11, 453–471. <https://doi.org/10.1007/s10950-007-9064-0>
- 893 28. García-Mayordomo, J., Insúa-Arévalo, J.M., Martínez-Díaz, J.J., Jiménez-Díaz, A.,
894 Álvarez-Gomez, J.A., Pérez-López, R., Rodríguez-Pascua, M.A., Martín-González, F.,
895 Giner-Robles, J., Masana, E., Nemser, E., Cabral, J., 2012. The Quaternary Active Faults

- 896 Database of Iberia v 0.1. *Journal of Iberian Geology* 38, 285–302.
897 https://doi.org/10.5209/rev_JIGE.2012.v38.n1.39219
- 898 29. García-Mayordomo, J., Martín-Banda, R., Insua-Arévalo, J.M., Álvarez-Gómez, J.A.,
899 Martínez-Díaz, J.J., Cabral, J., 2017. Active fault databases: Building a bridge between
900 earthquake geologists and seismic hazard practitioners, the case of the QAFI v.3 database.
901 *Natural Hazards and Earth System Sciences* 17, 1447–1459. [https://doi.org/10.5194/nhess-](https://doi.org/10.5194/nhess-17-1447-2017)
902 [17-1447-2017](https://doi.org/10.5194/nhess-17-1447-2017)
- 903 30. García-Mayordomo, J., Ortuño, M., Insua-Arévalo, J.M., Scotti, O., Visini, F., Fault2SHA-
904 Betics Working Group, 2018. The Fault2SHA-Betics Working Group: Promoting
905 knowledge interchange between earthquake geologists and seismic hazard modellers in the
906 Eastern Betics (SE Spain), in: *Resúmenes de La 3ª Reunión Ibérica Sobre Fallas Activas y*
907 *Paleosismología*, Alicante, España (2018). pp. 243–246.
- 908 31. Gaspar-Escribano, J.M., Benito, B., García-Mayordomo, J., 2008. Hazard-consistent
909 response spectra in the Region of Murcia (Southeast Spain): comparison to earthquake-
910 resistant provisions. *Bulletin of Earthquake Engineering* 6, 179–196.
- 911 32. Gaspar-Escribano, J.M., Rivas-Medina, A., Parra, H., Cabañas, L., Benito, B., Ruiz
912 Barajas, S., Martínez Solares, J.M., 2015. Uncertainty assessment for the seismic hazard
913 map of Spain. *Engineering Geology* 199, 62–73.
914 <https://doi.org/10.1016/j.enggeo.2015.10.001>
- 915 33. Gómez-Novell, O., Chartier, T., García-Mayordomo, J., Ortuño, M., Masana, E., Insua-
916 Arévalo, J.M., Scotti, O., 2019. Modelling earthquake multi-fault ruptures across complex
917 fault systems for probabilistic seismic hazard assessment: the Eastern Betics Shear Zone
918 [WWW Document]. Mendeley Data, v1. <https://doi.org/doi:10.17632/pt32rrncdm.1>
- 919 34. Gutenberg, B., Richter, C.F., 1944. Frequency of earthquakes in California. *Bulletin of the*
920 *Seismological Society of America* 34, 185–188.
- 921 35. Herrero-Barbero, P., 2016. Análisis estructural del segmento Alhama – Alcantarilla de la
922 Falla de Alhama de Murcia y sus implicaciones en el Riesgo Análisis estructural del
923 segmento Alhama – Alcantarilla de la Falla de Alhama de Murcia y sus implicaciones en el

- 924 Riesgo Sísmico . Universidad Complutense de Madrid.
- 925 36. Herrero-Barbero, P., Álvarez-Gómez, J.A., Martínez-Díaz, J.J., 2017. Análisis estructural
926 en el segmento Alhama de Murcia – Alcantarilla (Falla de Alhama de Murcia) y sus
927 implicaciones en la peligrosidad sísmica. *Geogaceta* 62, 11–14.
- 928 37. IGME, 2015a. QAFI v.3: Quaternary Active Faults Database of Iberia. [WWW Document].
929 URL <http://info.igme.es/qafi> (accessed 6.27.19).
- 930 38. IGME, 2015b. ZESIS: Base de Datos de Zonas Sismogénicas de la Península Ibérica y
931 territorios de influencia para el cálculo de la peligrosidad sísmica en España. [WWW
932 Document]. URL <http://info.igme.es/zesis> (accessed 6.27.19).
- 933 39. IGN-UPM working group, 2013. Actualización de mapas de peligrosidad sísmica de
934 España 2012. Centro Nacional de Información Geográfica, Instituto Geográfico Nacional,
935 Madrid.
- 936 40. Insua-Arévalo, J.M., García-Mayordomo, J., Salazar, A.E., Rodríguez-Escudero, E.,
937 Martín-Banda, R., Álvarez-Gómez, J.A., Canora, C., Martínez-Díaz, J.J., 2015.
938 Paleoseismological evidence of holocene activity of the los tollos fault (Murcia, SE Spain):
939 A lately formed quaternary tectonic feature of the eastern betic shear zone. *Journal of*
940 *Iberian Geology* 41, 333–350. https://doi.org/10.5209/rev_JIGE.2015.v41.n3.49948
- 941 41. Kearse, J., Little, T.A., Van Dissen, R.J., Barnes, P.M., Langridge, R., Mountjoy, J., Ries,
942 W., Villamor, P., Clark, K.J., Benson, A., Lamarche, G., Hill, M., Hemphill-Haley, M.,
943 2018. Onshore to offshore ground-surface and seabed rupture of the Jordan–Kekerengu–
944 Needles fault network during the 2016 Mw 7.8 Kaikoura earthquake, New Zealand.
945 *Bulletin of the Seismological Society of America* 108, 1573–1595.
946 <https://doi.org/10.1785/0120170304>
- 947 42. Langridge, R.M., Rowland, J., Villamor, P., Mountjoy, J., Townsend, D.B., Nissen, E.,
948 Madugo, C., Ries, W.F., Gasston, C., Canva, A., Hatem, A.E., Hamling, I., 2018.
949 Coseismic rupture and preliminary slip estimates for the Papatea fault and its role in the
950 2016 mw 7.8 Kaikōura, New Zealand, earthquake. *Bulletin of the Seismological Society of*
951 *America* 108, 1596–1622. <https://doi.org/10.1785/0120170336>

- 952 43. Leonard, M., 2010. Earthquake fault scaling: Self-consistent relating of rupture length,
953 width, average displacement, and moment release. *Bulletin of the Seismological Society of*
954 *America* 100, 1971–1988. <https://doi.org/10.1785/0120090189>
- 955 44. Little, T.A., van Dissen, R., Kearse, J., Norton, K., Benson, A., Wang, N., 2018.
956 Kekerengu fault, New Zealand: Timing and size of late holocene surface ruptures. *Bulletin*
957 *of the Seismological Society of America* 108, 1556–1572.
958 <https://doi.org/10.1785/0120170152>
- 959 45. Magrin, A., Peresan, A., Kronrod, T., Vaccari, F., Panza, G.F., 2017. Neo-deterministic
960 seismic hazard assessment and earthquake occurrence rate. *Engineering Geology* 229, 95–
961 109. <https://doi.org/10.1016/j.enggeo.2017.09.004>
- 962 46. Malservisi, R., Furlong, K.P., Gans, C.R., 2005. Microseismicity and creeping faults: Hints
963 from modeling the Hayward fault, California (USA). *Earth and Planetary Science Letters*
964 235, 421–435. <https://doi.org/10.1029/2000jb000084>
- 965 47. Martín-Banda, R., García-Mayordomo, J., Insua-Arévalo, J.M., Salazar, A.E., Rodríguez-
966 Escudero, E., Álvarez-Gómez, J.A., Medialdea, A., Herrero, M.J., 2015. New insights on
967 the seismogenic potential of the Eastern Betic Shear Zone (SE Iberia): Quaternary activity
968 and paleoseismicity of the SW segment of the Carrascoy Fault Zone. *Tectonics* 35, 55–75.
969 <https://doi.org/10.1002/2015TC003997>
- 970 48. Martínez-Díaz, J.J., 1998. Neotectónica y Tectónica Activa del Sector Centro-Occidental
971 de la Región de Murcia y Sur de Almería (Cordillera Bética – España). PhD thesis,
972 Universidad Complutense de Madrid, Madrid, Spain.
- 973 49. Martínez-Díaz, J.J., Alonso-Henar, J., Insua-Arévalo, J.M., Canora, C., García-
974 Mayordomo, J., Rodríguez-Escudero, E., Álvarez-Gómez, J.A., Ferrater, M., Ortuño, M.,
975 Masana, E., 2018. Geological evidences of surface rupture related to a seventeenth century
976 destructive earthquake in Betic Cordillera (SE Spain): constraining the seismic hazard of
977 the Alhama de Murcia fault. *Journal of Iberian Geology*. [https://doi.org/10.1007/s41513-](https://doi.org/10.1007/s41513-018-0082-2)
978 [018-0082-2](https://doi.org/10.1007/s41513-018-0082-2)
- 979 50. Martínez-Díaz, J.J., Bejar-Pizarro, M., Álvarez-Gómez, J.A., Mancilla, F.L., Stich, D.,

- 980 Herrera, G., Morales, J., 2012a. Tectonic and seismic implications of an intersegment
981 rupture. The damaging May 11th 2011 Mw 5.2 Lorca, Spain, earthquake. *Tectonophysics*
982 546–547, 28–37. <https://doi.org/10.1016/j.tecto.2012.04.010>
- 983 51. Martínez-Díaz, J.J., Masana, E., Hernández-Enrile, J.L., Santanach, P., 2003. Effects of
984 repeated paleoearthquakes on the Alhama de Murcia Fault (Betic Cordillera , Spain) on
985 the Quaternary evolution of an alluvial fan system. *Annals of Geophysics* 46, 775–791.
986 <https://doi.org/10.4401/ag-3455>
- 987 52. Martínez-Díaz, J.J., Masana, E., Ortuño, M., 2012b. Active tectonics of the Alhama de
988 Murcia fault, Betic Cordillera, Spain. *Journal of Iberian Geology* 38, 253–270.
989 https://doi.org/10.5209/rev_JIGE.2012.v38.n1.39218
- 990 53. Masana, E., Martínez-Díaz, J.J., Hernández-Enrile, J.L., Santanach, P., 2004. The Alhama
991 de Murcia fault (SE Spain), a seismogenic fault in a diffuse plate boundary: Seismotectonic
992 implications for the Ibero-Magrebic region. *Journal of Geophysical Research: Solid Earth*
993 109, 1–17. <https://doi.org/10.1029/2002JB002359>
- 994 54. Masana, E., Moreno, X., Gràcia, E., Pallàs, R., Ortuño, M., López, R., Gómez-Novell, O.,
995 Ruano, P., Perea, H., Štěpančíková, P., Khazaradze, G., 2018. First evidence of
996 paleoearthquakes along the Carboneras Fault Zone (SE Iberian Peninsula): Los Trances
997 site. *Geologica Acta* 16, 461–476. <https://doi.org/10.1344/GeologicaActa2018.16.4.8>
- 998 55. McCalpin, J., 1996. *Paleoseismology*. Academic Press.
- 999 56. McGuire, R.K., 1976. *EQRISK Evaluation of Sites for Earthquake Risk*. USGS Open-File
1000 Report 76-67.
- 1001 57. Moreno, X., 2011. *Neotectonic and Paleoseismic Onshore-Offshore integrated study of the*
1002 *Carboneras Fault (Eastern Betics, SE Iberia)*. PhD thesis, Universitat de Barcelona,
1003 Barcelona, Spain.
- 1004 58. Moreno, X., Masana, E., Pallàs, R., Gràcia, E., Rodés, Á., Bordonau, J., 2015. Quaternary
1005 tectonic activity of the Carboneras Fault in the La Serrata range (SE Iberia):
1006 Geomorphological and chronological constraints. *Tectonophysics* 663, 78–94.
1007 <https://doi.org/10.1016/j.tecto.2015.08.016>

- 1008 59. Ortuño, M., Masana, E., García-Meléndez, E., Martínez-Díaz, J.J., Štěpančíková, P.,
1009 Cunha, P.P., Sohbatí, R., Canora, C., Buylaert, J.P., Murray, A.S., 2012. An exceptionally
1010 long paleoseismic record of a slow-moving fault: The Alhama de Murcia fault (Eastern
1011 Betic shear zone, Spain). *Bulletin of the Geological Society of America* 124, 1474–1494.
1012 <https://doi.org/10.1130/B30558.1>
- 1013 60. Pedrera, A., Galindo-Zaldívar, J., Marín-Lechado, C., García-Tortosa, F.J., Ruano, P.,
1014 Garrido, A.C., Azañón, J.M., Peláez, J.A., Giaconia, F., 2012. Recent and active faults and
1015 folds in the central-eastern Internal Zones of the Betic Cordillera. *Journal of Iberian*
1016 *Geology* 38, 191–208. https://doi.org/10.5209/rev_JIGE.2012.v38.n1.39213
- 1017 61. Peláez, J.A., Delgado, J., López Casado, C., 2005. A preliminary probabilistic seismic
1018 hazard assessment in terms of Arias intensity in southeastern Spain. *Engineering Geology*
1019 77, 139–151. <https://doi.org/10.1016/j.enggeo.2004.09.002>
- 1020 62. Rastgoo, M., Rahimi, H., Romanelli, F., Vaccari, F., Panza, G.F., 2018. Neo-deterministic
1021 seismic hazard assessment for Alborz Region, Iran. *Engineering Geology* 242, 70–80.
1022 <https://doi.org/10.1016/j.enggeo.2018.05.025>
- 1023 63. Rivas-Medina, A., Benito, B., Miguel Gaspar-Escribano, J., 2018. Approach for combining
1024 fault and area sources in seismic hazard assessment: Application in south-eastern Spain.
1025 *Natural Hazards and Earth System Sciences* 18, 2809–2823. [https://doi.org/10.5194/nhess-](https://doi.org/10.5194/nhess-18-2809-2018)
1026 [18-2809-2018](https://doi.org/10.5194/nhess-18-2809-2018)
- 1027 64. Roquero, E., Silva, P.G., Rodríguez-Pascua, M.A., Bardají, T., Elez, J., Carrasco-García,
1028 P., Giner-Robles, J.L., 2019. Analysis of faulted fan surfaces and paleosols in the
1029 Palomares Fault Zone (Betic Cordillera, SE Spain): Paleoclimatic and paleoseismic
1030 implications. *Geomorphology* 342, 88–102.
1031 <https://doi.org/10.1016/j.geomorph.2019.06.003>
- 1032 65. Scholz, C.H., 1990. *The mechanics of earthquakes and faulting*. Cambridge University
1033 Press, Cambridge, United Kingdom. <https://doi.org/10.1017/9781316681473>
- 1034 66. Schwartz, D.P., 2018. Review: Past and future fault rupture lengths in seismic source
1035 characterization-the long and short of it. *Bulletin of the Seismological Society of America*

- 1036 108, 2493–2520. <https://doi.org/10.1785/0120160110>
- 1037 67. Schwartz, D.P., Coppersmith, K.J., 1984. Fault behavior and characteristic earthquakes:
1038 Examples from the Wasatch and San Andreas Fault Zones 89, 5681–5698.
- 1039 68. Shen, Z.K., Jackson, D.D., Feng, Y.J., Cline, M., Kim, M., Fang, P., Bock, Y., 1994.
1040 Postseismic Deformation Following the Landers Earthquake, California, 28 June 1992.
1041 Bulletin of the Seismological Society of America 84, 780–791.
1042 <https://doi.org/10.1029/97JB00210>
- 1043 69. Silva, P.G., Goy, J.L., Somoza, L., Zazo, C., Bardají, T., 1993. Landscape response to
1044 strike-slip faulting linked to collisional settings: Quaternary tectonics and basin formation
1045 in the Eastern Betics, southeastern Spain. Tectonophysics 224, 289–303.
1046 [https://doi.org/10.1016/0040-1951\(93\)90034-H](https://doi.org/10.1016/0040-1951(93)90034-H)
- 1047 70. Stein, R.S., Lisowski, M., 1983. The 1979 Homestead Valley Earthquake Sequence,
1048 California: Control of aftershocks and postseismic deformation. Journal of Geophysical
1049 Research: Solid Earth 88, 6477–6490.
- 1050 71. Stich, D., Martín, J.B., Morales, J., 2007. Deformación sísmica y asísmica en la zona
1051 Béticas-Rif-Alborán. Revista de la Sociedad Geológica de España 20, 311–320.
- 1052 72. Stich, D., Martín, R., Morales, J., 2010. Moment tensor inversion for Iberia-Maghreb
1053 earthquakes 2005–2008. Tectonophysics 483, 390–398.
1054 <https://doi.org/10.1016/j.tecto.2009.11.006>
- 1055 73. Stirling, M., Gerstenberger, M., 2018. Applicability of the Gutenberg-Richter relation for
1056 major active faults in New Zealand. Bulletin of the Seismological Society of America 108,
1057 718–728. <https://doi.org/10.1785/0120160257>
- 1058 74. Valentini, A., Visini, F., Pace, B., 2017. Integrating faults and past earthquakes into a
1059 probabilistic seismic hazard model for peninsular Italy. Natural Hazards and Earth System
1060 Sciences 17, 2017–2039. <https://doi.org/10.5194/nhess-17-2017-2017>
- 1061 75. Wang, J.P., Lin, C.W., Taheri, H., Chan, W.S., 2012. Impact of fault parameter
1062 uncertainties on earthquake recurrence probability examined by Monte Carlo simulation -
1063 an example in Central Taiwan. Engineering Geology 126, 67–74.

- 1064 <https://doi.org/10.1016/j.enggeo.2011.12.012>
- 1065 76. Wei, S., Fielding, E., Leprince, S., Sladen, A., Avouac, J.P., Helmberger, D., Hauksson, E.,
1066 Chu, R., Simons, M., Hudnut, K., Herring, T., Briggs, R., 2011. Superficial simplicity of
1067 the 2010 El Mayorg-Cucapah earthquake of Baja California in Mexico. *Nature Geoscience*
1068 4, 615–618. <https://doi.org/10.1038/ngeo1213>
- 1069 77. Wells, D.L., Coppersmith, K.J., 1994. New empirical relationships among magnitude,
1070 rupture length, rupture width, rupture area, and surface displacements. *Bulletin of the*
1071 *Seismological Society of America* 84, 974–1002.
- 1072 78. Wesnousky, S.G., 2008. Displacement and geometrical characteristics of earthquake
1073 surface ruptures: Issues and implications for seismic-hazard analysis and the process of
1074 earthquake rupture. *Bulletin of the Seismological Society of America* 98, 1609–1632.
1075 <https://doi.org/10.1785/0120070111>
- 1076 79. Wesnousky, S.G., 1986. Earthquakes, Quaternary Faults, and Seismic Hazard in California.
1077 *Journal of Geophysical Research* 91, 12,587-12,631.
1078 <https://doi.org/10.1029/JB091iB12p12587>
- 1079 80. Woessner, J., Laurentiu, D., Giardini, D., Crowley, H., Cotton, F., Grünthal, G., Valensise,
1080 G., Arvidsson, R., Basili, R., Demircioglu, M.B., Hiemer, S., Meletti, C., Musson, R.W.,
1081 Rovida, A.N., Sesetyan, K., Stucchi, M., 2015. The 2013 European Seismic Hazard Model:
1082 key components and results. *Bulletin of Earthquake Engineering* 13, 3553–3596.
1083 <https://doi.org/10.1007/s10518-015-9795-1>
- 1084 81. Working Group On California Earthquake Probabilities, 2003. *Earthquake Probabilities in*
1085 *the San Francisco Bay Region : 2002-2031*, USGS Open-File Report 03-214.
- 1086 82. Youngs, R.R., Coppersmith, K.J., 1985. Implications of fault slip rates and earthquake
1087 recurrence models to probabilistic seismic hazard estimates. *International Journal of Rock*
1088 *Mechanics and Mining Sciences & Geomechanics Abstracts* 23, 125.
1089 [https://doi.org/10.1016/0148-9062\(86\)90651-0](https://doi.org/10.1016/0148-9062(86)90651-0)
- 1090

1091 **Figure captions**

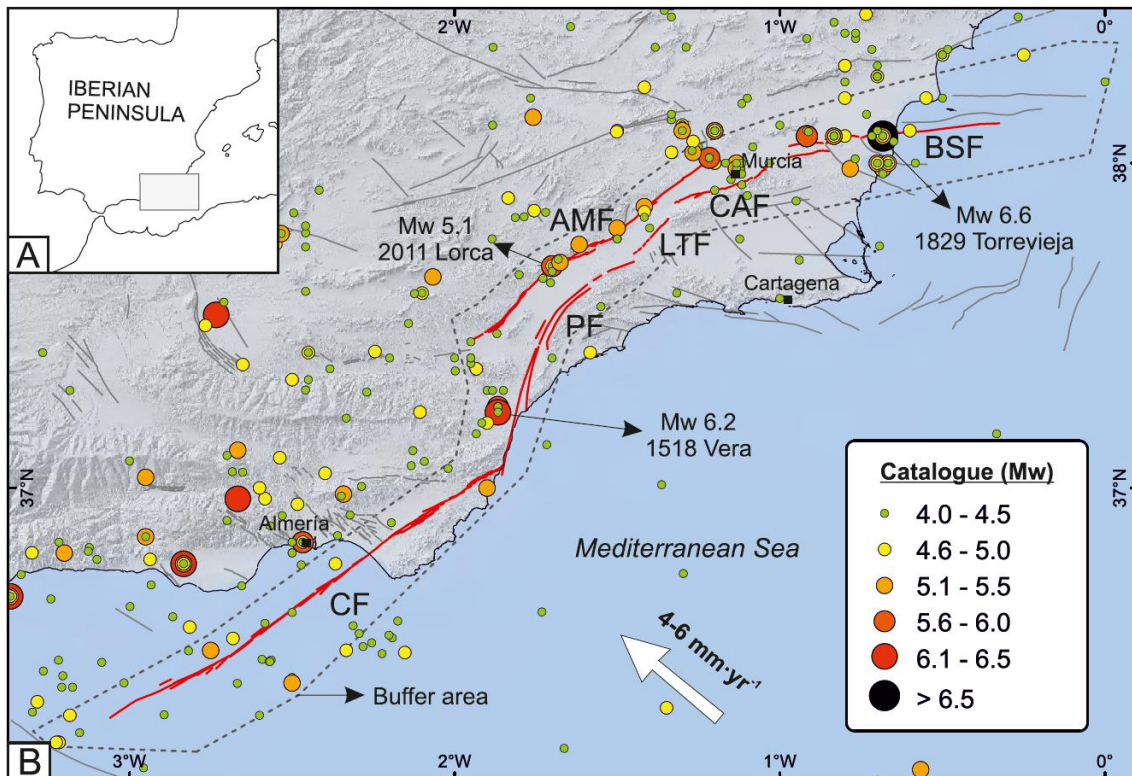
1092 Figure 1. A. Location of the study area within the Iberian Peninsula. B. Tectonic scheme
1093 of the Eastern Betics Shear Zone (EBSZ). Faults considered in the present study are
1094 depicted in red. CF: Carboneras fault; PF: Palomares fault; LTF: Los Tollos fault; CAF:
1095 Carrascoy fault; BSF: Bajo Segura fault; AMF: Alhama de Murcia fault. The time period
1096 covered by the earthquake catalogue extends from years 1048 to 2011 (IGN-UPM
1097 working group, 2013). The largest known historical and instrumental earthquakes within
1098 the buffer area are pointed with an arrow (Requires color online only; target size: 1.5
1099 columns).

1100 Figure 2. A. Simplified fault traces of the main active faults in the EBSZ used in this
1101 study (extracted from the Quaternary Active Faults Database of Iberia; IGME, 2015a)
1102 and sections defined for each one of the major faults. Each fault section is codified with
1103 an ID corresponding to the abbreviation of the fault and the number of the section (see
1104 table 1 for the assignation of the section ID to major faults). The extension of the
1105 maximum fault ruptures allowed in each rupture hypothesis is shown. B. Slip rate ranges
1106 of the EBSZ faults depicted following a colored scale. The buffer area considered is
1107 indicated. (Requires color in print; target size: 1.5 columns).

1108 Figure 3. Comparison between the GR curves modelled with SHERIFS for each
1109 hypothesis (grey) and the earthquake rates from the catalogue (point cloud). Mean GR
1110 curve modelled: solid black line; samples modelled: short grey lines; mean GR curve of
1111 the catalogue: dashed line. The bottom of the hyp. 1 graph shows the cumulative number
1112 of earthquakes of the catalogue per magnitude used to draw its MFD. Non-Main-Shock
1113 slip (NMS) histograms of the resulting models are indicated. (Requires color online only;
1114 target size: 1.5 columns).

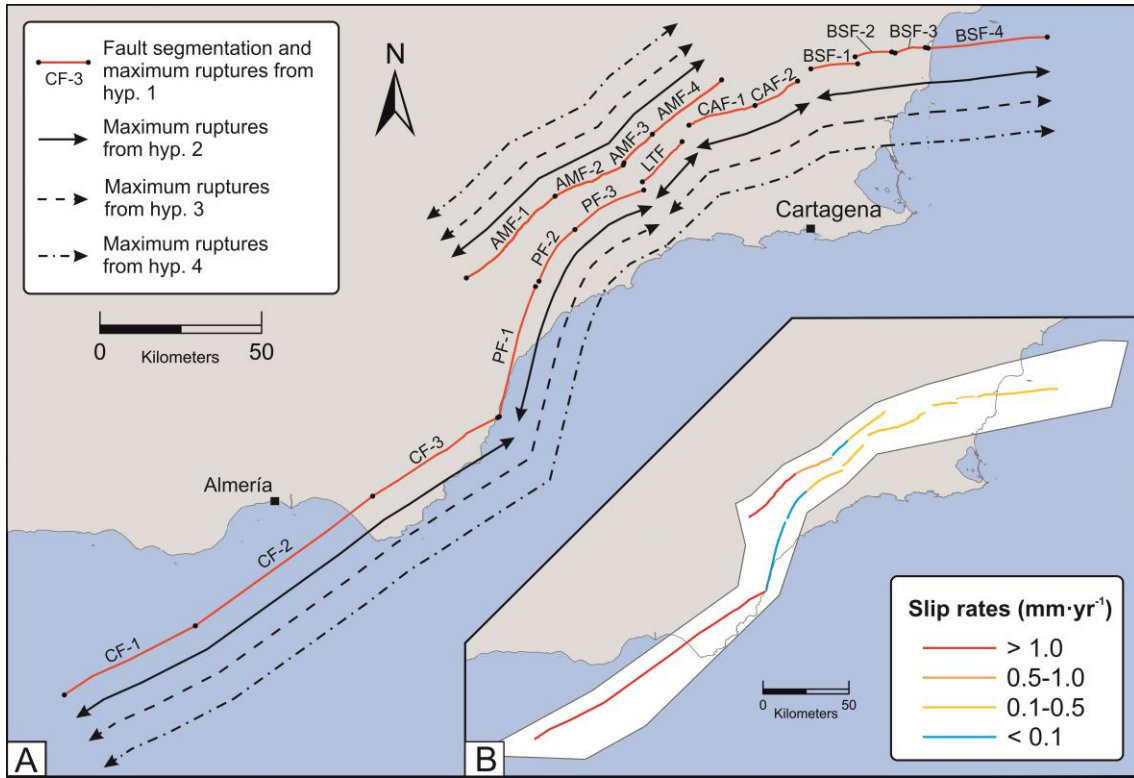
1115 Figure 4. Annual rates of paleoearthquakes with their uncertainty ranges inferred from
1116 paleoseismological studies. These are plotted together with the modelled GR curves of
1117 their respective fault sections (participation rates) and for each rupture hypothesis. A fault
1118 map with the location of the paleoseismic studies (numbers) in each fault section is
1119 included. 1: Ferrater (2016); 2: Martínez-Díaz et al. (2018); 3: Ortuño et al. (2012); 4:
1120 Moreno (2011); 5: Insua-Arévalo et al. (2015); 6: Martín-Banda et al. (2015).
1121 Paleoearthquake rate values are available in table 2. (Requires color online only; target
1122 size: double column).

1123 **Figure 1**



1124

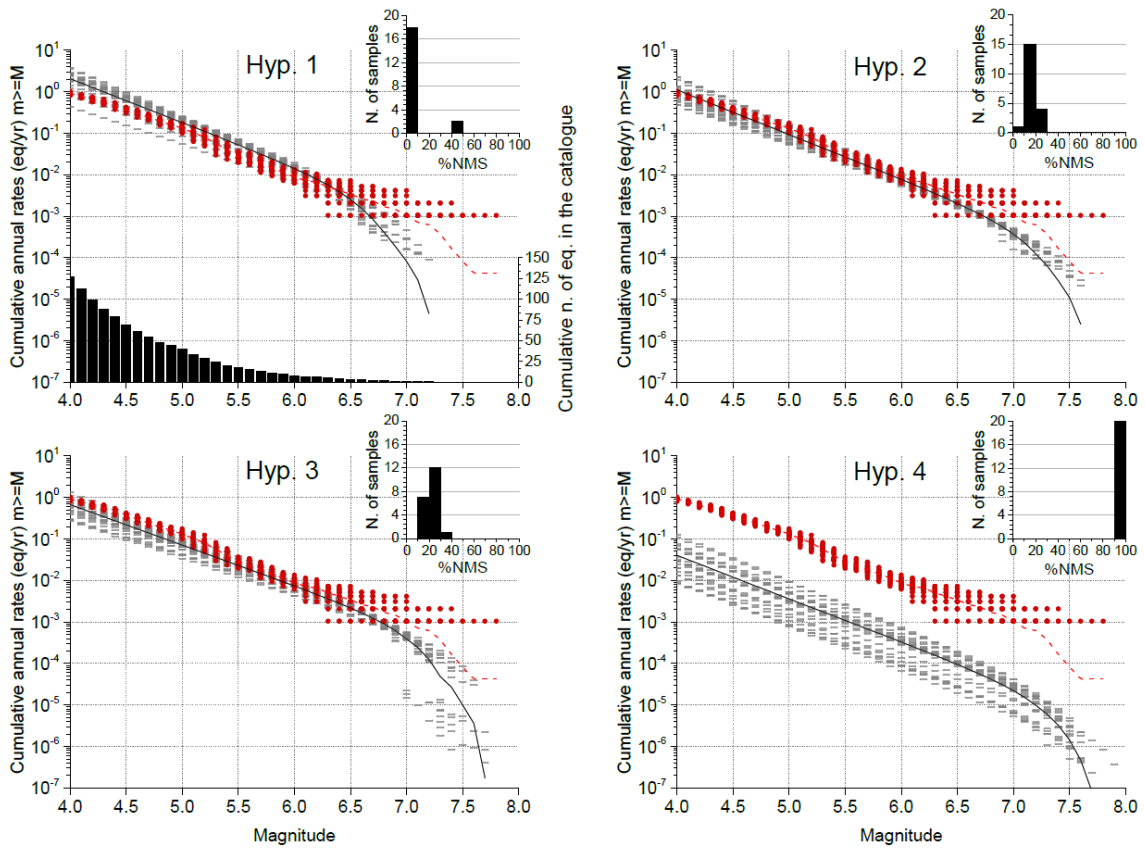
Figure 2



1125

1126

Figure 3



1127

Figure 4

